

TUM-T31-67/94/R
 MPI-PhT/94-49/R
 UAB-FT-347/R
 hep-ph/9408306

Charm Quark Mass Dependence of QCD Corrections to Nonleptonic Inclusive B Decays

E. Bagan^{1*}, Patricia Ball^{2†}, V.M. Braun^{3‡} and P. Gosdzinsky⁴

¹*Physics Department, Brookhaven National Laboratory, Upton, NY 11973, USA*

²*Physik-Department/T30, TU München, D-85747 Garching, Germany*

³*Max-Planck-Institut für Physik, P.O. Box 40 12 12, D-80805 München, Germany*

⁴*Grup de Física Teòrica, Dept. de Física and Institut de Física d'Altes Energies, IFAE, Universitat Autònoma de Barcelona, E-08193 Bellaterra (Barcelona), Spain*

September 6, 1994

Abstract:

We calculate the radiative corrections to the nonleptonic inclusive B decay mode $b \rightarrow c\bar{u}d$ taking into account the charm quark mass. Compared to the massless case, corrections resulting from a nonvanishing c quark mass increase the nonleptonic rate by (4–8)%, depending on the renormalization point. As a by-product of our calculation, we obtain an analytic expression for the radiative correction to the semileptonic decay $b \rightarrow u\tau\bar{\nu}$ taking into account the τ lepton mass, and estimate the c quark mass effects on the nonleptonic decay mode $b \rightarrow c\bar{c}s$.

To appear in Nucl. Phys. B

*Permanent address: Grup de Física Teòrica, Dept. de Física and Institut de Física d'Altes Energies, IFAE, Universitat Autònoma de Barcelona, E-08193 Bellaterra (Barcelona), Spain

†Address after September 1994: CERN, Theory Division, CH-1211 Genève 23, Switzerland

‡Address after August 1994: DESY, Notkestraße 85, D-22603 Hamburg, Germany

1 Introduction

The past few years have witnessed a continuous interest in the physics of heavy quarks, in particular B meson decays. In addition to their potential rôle as precision tests of the Standard Model, they also provide important information on the Cabibbo–Kobayashi–Maskawa (CKM) matrix elements V_{cb} , V_{bu} , and others. From a theoretical point of view, inclusive widths tend generally to be cleaner than exclusive ones. This is in particular true for the decays of heavy hadrons, which are essentially short distance processes since the amount of energy released is large compared with a typical confinement scale of ~ 1 GeV. Indeed it can be shown, cf. [1, 2], that up to corrections of order $1/m_b^2$, m_b being the b quark mass, inclusive decay rates of beautiful hadrons are essentially the same as for the underlying quark processes and thus can reliably be calculated in perturbation theory. Moreover, the corrections suppressed by powers of the heavy quark mass can be evaluated in a systematic way, using the operator product expansion (OPE) technique combined with the heavy quark expansion [1, 2]. At present, it is widely believed that inclusive decay widths — semileptonic, rare radiative or hadronic — may be reliably predicted to an accuracy limited mainly by the unavoidable shortcomings of perturbative calculations such as scale- and scheme-dependence. There is little controversy that these calculations rest on a firm theoretical foundation.

A high accuracy thus requires the calculation of radiative corrections to inclusive widths, a task pioneered by the authors of [3], where the radiative correction to the semileptonic decay width of the D meson was obtained from earlier calculations [4] of the muon decay in QED. At present, $\mathcal{O}(\alpha_s)$ corrections are known for both the semileptonic and the hadronic decay width [5, 6], in the approximation of massless final state quarks.

Taking into account the masses of the final state particles has proved to be a difficult task. A significant effort in this direction has been made by Hokim and Pham [7], who calculated one-gluon corrections to inclusive weak decays taking full account of all the masses. Nir [8] has further found an analytical expression for the radiative correction to the semileptonic $b \rightarrow ce\bar{\nu}$ decay, the numerical results being given in [3]. Unfortunately, the results of [7] are not sufficient for the calculation of inclusive widths with renormalization group improvement to two-loop accuracy, since in addition to the α_s correction calculated by Hokim and Pham one must take into account terms proportional to $\alpha_s^2 \ln M_W^2/m_b^2$ which are equally important and are also in general mass-dependent. Thus, in practice of data analysis quark mass corrections to nonleptonic decays are generally being omitted. On the other hand, it is known that the effect of non-zero masses on the radiative corrections can be very large, especially if they involve colour-attraction in the final state. An example was provided recently within the heavy quark effective theory: radiative corrections to correlation functions, containing one heavy and one light quark and evaluated near the mass-shell of the heavy quark, turned out to be by almost an order of magnitude larger than for light quarks [9]. Thus the actual size of radiative corrections in nonleptonic decays is essentially not fixed and deserves a detailed study. We address this problem in the present paper.

Apart from the pursuit of completeness of formulas, our study has been fuelled by

an intriguing conflict of theory with experiment, concerning the semileptonic branching ratio of the B meson: over the last few years the measured semileptonic branching ratio [10] has consistently turned out to be (15–20)% smaller than theoretical expectations, and the reason for this discrepancy is not understood. This problem has attracted already considerable attention among theorists [11, 12, 13, 14]. We believe that the knowledge of radiative corrections to nonleptonic decays with full account for the c quark mass is imperative for a quantitative understanding of the problem.

A principal new result of this paper is the calculation of the QCD radiative correction to the inclusive decay mode

- $b \rightarrow c\bar{u}d$

including full dependence on the c quark mass and the renormalization group improvement to the two-loop accuracy. This decay dominates the hadronic B meson width and is crucial for understanding the semileptonic branching ratio. We complete the calculations of [7] by studying relevant corrections due to operator-mixing and obtain analytic expressions for all radiative corrections with one massive quark in the final state, which so far have partly been only available in form of one-dimensional parametric integrals [7]. As a by-product of this analysis, we obtain an analytic expression for radiative corrections to the decay

- $b \rightarrow u\tau\bar{\nu}$

taking into account the τ lepton mass. Decays involving the τ leptons are potentially very interesting, since they may be used to constrain certain extensions of the Standard Model and attract an ever increasing experimental and theoretical interest [15].

In addition, we estimate QCD corrections to the decay

- $b \rightarrow c\bar{c}s$,

considering the colour-favoured contribution, and argue that in this case the radiative correction is strongly enhanced when the c quark mass is included. When appropriate, we compare our results with those of Hokim and Pham.

With realistic values of the b and c quark masses, the nonleptonic rate $b \rightarrow c\bar{u}d$ is increased by approximately (4–8)%, depending on the renormalization scale, if a non-zero c quark mass is taken into account which has to be compared with a (4–7)% increase for the semileptonic $b \rightarrow ce\bar{\nu}$ rate. Thus, the ratio $\Gamma(b \rightarrow cud)/\Gamma(b \rightarrow ce\bar{\nu})$ is only weakly affected by taking into account the c quark mass in the radiative corrections. This compensation is due to the specific structure of the effective weak Lagrangian, which suppresses the gluon exchange between the c and the light quarks. The τ lepton mass corrections to the decay $b \rightarrow u\tau\bar{\nu}$ turn out to be of the same order of magnitude as c quark mass corrections to the semileptonic $b \rightarrow ce\bar{\nu}$ decay.

Although the calculations are straightforward in principle, in practice they turn out to be rather tedious and involve several delicate points which we discuss in detail below. We use a conservative technique and calculate total imaginary parts by means of Cutkosky rules, i.e. we sum up contributions corresponding to real and virtual gluon emission, and

introduce small masses for the gluon and the light quark to avoid infra-red (IR) divergences due to the presence of massless particles in the final state. The virtual corrections are calculated using dimensional regularization, a framework that requires special care with the definition of the γ_5 matrix. We use the so-called naïve dimensional regularization (NDR) scheme, in which γ_5 anticommutes in D dimensions. This scheme has been shown to yield correct results for the two-loop anomalous dimensions in the relevant terms of the effective weak Lagrangian [16]. In the limit of zero masses of all final state particles our results coincide with those of Altarelli et al., [5], obtained in the dimensional reduction scheme, and with those of Buchalla, [6], obtained in the 't Hooft–Veltman scheme.

Our paper is organized as follows: in Sec. 2 we recall the general framework for the calculation of weak processes to next-to-leading order in QCD, list the necessary contributions to be calculated, explain the particular calculation procedure which we use throughout this paper, and discuss various subtle points. Sec. 3 contains our main results: the analytic expressions for the radiative corrections for non-zero c quark (τ lepton) mass, along with simple parametrizations. In Sec. 4 we estimate the effect of finite mass corrections on the decay $b \rightarrow c\bar{c}s$. Sec. 5 contains the numerical analysis and a discussion of various phenomenological applications. Sec. 6 completes the paper with a summary and conclusions. Technical details of the calculation are given in the appendices.

2 Theoretical Framework

This section is mainly introductory. We collect the necessary definitions and describe the main steps in the calculation of inclusive decay widths to next-to-leading order.

2.1 The Effective Lagrangian

Let us consider a Standard Model nonleptonic weak process induced by charged currents. In the limit of infinite W boson mass m_W and to leading order in the weak coupling, the charm-changing nonleptonic decays of beautiful particles can be described by the effective Lagrangian

$$\begin{aligned} \mathcal{L}_{\text{eff}}^{\Delta C=1} = & -\frac{G_F}{\sqrt{2}} V_{ud}^* V_{cb} \{C_1(\mu) \mathcal{O}_1(\mu) + C_2(\mu) \mathcal{O}_2(\mu)\} \\ & -\frac{G_F}{\sqrt{2}} V_{us}^* V_{cb} \{C_1(\mu) \mathcal{O}'_1(\mu) + C_2(\mu) \mathcal{O}'_2(\mu)\}. \end{aligned} \quad (2.1)$$

Here \mathcal{O}_2 is the colour-singlet operator

$$\mathcal{O}_2 = (\bar{d}u)_{V-A} (\bar{c}b)_{V-A} \quad (2.2)$$

appearing in the tree-level Lagrangian, whereas the non-singlet operator (α and β are colour-indices)

$$\mathcal{O}_1 = (\bar{d}_\alpha u_\beta)_{V-A} (\bar{c}_\beta b_\alpha)_{V-A} \quad (2.3)$$

is generated by the strong interaction. The operators \mathcal{O}'_i are obtained from the \mathcal{O}_i by the replacement $\bar{d} \rightarrow \bar{s}$. The Wilson-coefficients $C_i(\mu)$ can be calculated at the scale $\mu = m_W$ and then evolved down to scales $\mu \ll m_W$ by solving the corresponding renormalization group equations. Since the operators \mathcal{O}_1 and \mathcal{O}_2 mix under renormalization, it is convenient to introduce the operators $\mathcal{O}_\pm = (\mathcal{O}_2 \pm \mathcal{O}_1)/2$ which renormalize multiplicatively.¹ To two-loop accuracy, the corresponding Wilson-coefficients are given by [5, 16]

$$C_\pm(\mu) = C_2(\mu) \pm C_1(\mu) \\ = L_\pm(\mu) \left\{ 1 + \frac{\alpha_s(m_W) - \alpha_s(\mu)}{4\pi} \frac{\gamma_\pm^{(0)}}{2\beta_0} \left(\frac{\gamma_\pm^{(1)}}{\gamma_\pm^{(0)}} - \frac{\beta_1}{\beta_0} \right) + \frac{\alpha_s(m_W)}{4\pi} B_\pm \right\}. \quad (2.4)$$

Here

$$L_\pm(\mu) = \left[\frac{\alpha_s(m_W)}{\alpha_s(\mu)} \right]^{\gamma_\pm^{(0)}/(2\beta_0)} \quad (2.5)$$

is the solution of the renormalization group equation for C_\pm to leading logarithmic order, whereas the term proportional to $\alpha_s(m_W) - \alpha_s(\mu)$ takes into account the renormalization group improvement to next-to-leading order. The $\gamma_\pm^{(i)}$ are the coefficients of the anomalous dimensions of the operators \mathcal{O}_\pm and \mathcal{O}'_\pm ,

$$\gamma_\pm = \gamma_\pm^{(0)} \frac{\alpha_s}{4\pi} + \gamma_\pm^{(1)} \left(\frac{\alpha_s}{4\pi} \right)^2 + \mathcal{O}(\alpha_s^3), \quad (2.6)$$

with [16]

$$\gamma_+^{(0)} = 4, \quad \gamma_-^{(0)} = -8, \quad \gamma_+^{(1)} = -7 + \frac{4}{9} n_f, \quad \gamma_-^{(1)} = -14 - \frac{8}{9} n_f \quad (2.7)$$

in naïve dimensional regularization with anticommuting γ_5 and n_f running flavours (five in our case). The β_i are the first two coefficients of the QCD β -function,

$$\beta = -g_s \left\{ \beta_0 \frac{\alpha_s}{4\pi} + \beta_1 \left(\frac{\alpha_s}{4\pi} \right)^2 + \mathcal{O}(\alpha_s^3) \right\}, \\ \beta_0 = 11 - \frac{2}{3} n_f, \quad \beta_1 = 102 - \frac{38}{3} n_f. \quad (2.8)$$

Finally, the B_\pm are the matching coefficients ensuring that up to terms of order $\alpha_s^2(m_W)$, matrix elements of the effective Lagrangian calculated at the scale $\mu = m_W$ equal the corresponding matrix elements calculated with the full standard model Lagrangian. Fierz-symmetry implies

$$B_\pm = \pm B \frac{N_c \mp 1}{2N_c}, \quad (2.9)$$

¹Hereafter we imply that the renormalization scheme obeys Fierz-symmetry. Within dimensional regularization this requires certain restrictions on the particular choice of the so-called evanescent operators, see [16, 17, 18].

where $N_c = 3$ is the number of colours. In the NDR scheme one finds [16]

$$B = 11. \quad (2.10)$$

Note that both the matching coefficients and the two-loop anomalous dimensions depend on the renormalization scheme. It proves, however, feasible to combine them into the scheme-independent quantity [5, 6, 16]

$$R_{\pm} = B_{\pm} + \frac{\gamma_{\pm}^{(0)}}{2\beta_0} \left(\frac{\gamma_{\pm}^{(1)}}{\gamma_{\pm}^{(0)}} - \frac{\beta_1}{\beta_0} \right),$$

$$R_+ = \frac{10863 - 1278n_f + 80n_f^2}{6(33 - 2n_f)^2}, \quad R_- = -\frac{15021 - 1530n_f + 80n_f^2}{3(33 - 2n_f)^2}, \quad (2.11)$$

in terms of which the Wilson-coefficients read

$$C_{\pm}(\mu) = L_{\pm}(\mu) \left\{ 1 + \frac{\alpha_s(m_W) - \alpha_s(\mu)}{4\pi} R_{\pm} + \frac{\alpha_s(\mu)}{4\pi} B_{\pm} \right\}. \quad (2.12)$$

In this form, all the remaining scheme-dependence is absorbed in B_{\pm} and is to be cancelled by the scheme-dependence of matrix elements of the corresponding operators.

2.2 The Inclusive Decay Rate

The total inclusive decay rate of a B meson into hadrons X_c , corresponding to the elementary subprocess $b \rightarrow c\bar{u}d + c\bar{u}s$, can be expressed as the imaginary part of a transition operator:

$$\Gamma(B \rightarrow X_c) = \frac{\pi}{m_B} \sum_n \int \prod_{i=1}^n \left[\frac{d^3 p_i}{(2\pi)^3 2E_i} \right] (2\pi)^3 \delta^4(p_B - \sum_i p_i) \left| \langle n | \mathcal{L}_{\text{eff}}^{\Delta C=1} | B \rangle \right|^2$$

$$= \frac{1}{m_B} \text{Im} \int d^4 x \langle B | T [\mathcal{L}_{\text{eff}}^{\Delta C=1}]^{\dagger}(x) \mathcal{L}_{\text{eff}}^{\Delta C=1}(0) | B \rangle \quad (2.13)$$

where the sum runs over all possible final states. Starting from this expression, it can be shown that in the limit of infinite b quark mass the B meson decay rate coincides with the decay rate of a free b quark, which can be calculated perturbatively. Recently, much attention has been paid to understand the structure of nonperturbative corrections to that simple picture which are suppressed by powers of the b quark mass [1, 2]. Yet in this paper we mainly address the question of how to calculate radiative corrections to the quark level decay and thus we proceed in a purely perturbative framework.

Summing over the squares of the relevant elements of the CKM matrix and making use of its approximate unitarity in the first two generations, the hadronic decay width is equal to the width of the semileptonic decay $b \rightarrow ce\bar{\nu}$,

$$\Gamma_0 = \frac{G_F^2 m_b^5}{192\pi^3} |V_{cb}|^2 f_1(m_c^2/m_b^2), \quad (2.14)$$

multiplied by a colour factor 3 and up to radiative corrections. Here we have neglected the light quark masses and the strange quark mass and introduced the notation $f_1(a)$ for the tree-level phase-space factor:

$$f_1(a) = 1 - 8a + 8a^3 - a^4 - 12a^2 \ln a. \quad (2.15)$$

By the quark masses m_b and m_c we hereafter understand the pole masses.

The expression for the inclusive decay width becomes more complicated if one turns on the renormalization group running of the Wilson-coefficients in the effective Lagrangian and calculates radiative corrections. To next-to-leading order accuracy one has to take into account the set of diagrams shown in Fig. 1. For practical calculations it proves convenient to split off the colour algebra and trivial multiplicative factors. Then the operators \mathcal{O}_1 and \mathcal{O}_2 become identical and the four-fermion vertices in Fig. 1 can be interpreted as insertions of $\mathcal{O} = (\bar{d}u)_{V-A}(\bar{c}b)_{V-A}$ or $(\bar{s}u)_{V-A}(\bar{c}b)_{V-A}$ where *no* summation over colour is implied. For definiteness, the diagrams in Fig. 1 represent the corresponding contribution of

$$i \int d^4x \langle b | T[\mathcal{O}^\dagger(x) \mathcal{O}(0)] | b \rangle_{\text{spin-averaged}} \quad (2.16)$$

to the forward-scattering amplitude for an on-shell b quark. The colour-factors of each diagram are given in Tab. 1.

Taking everything together, we can express the decay rate for $b \rightarrow c\bar{u}d + c\bar{u}s$ as

$$\begin{aligned} \Gamma(b \rightarrow c\bar{u}d + c\bar{u}s) = \Gamma_0 \left[2L_+^2(\mu) + L_-^2(\mu) + \frac{\alpha_s(m_W) - \alpha_s(\mu)}{2\pi} \{ 2L_+^2(\mu)R_+ + L_-^2(\mu)R_- \} \right. \\ + \frac{\alpha_s(\mu)}{2\pi} \{ 2L_+^2(\mu)B_+ + L_-^2(\mu)B_- \} \\ + \frac{3}{4} \{ L_+(\mu) + L_-(\mu) \}^2 \frac{2}{3} \frac{\alpha_s(\mu)}{\pi} \{ G_a + G_b \} \\ + \frac{3}{4} \{ L_+(\mu) - L_-(\mu) \}^2 \frac{2}{3} \frac{\alpha_s(\mu)}{\pi} \{ G_c + G_d \} \\ \left. + \frac{1}{2} \{ L_+^2(\mu) - L_-^2(\mu) \} \frac{2}{3} \frac{\alpha_s(\mu)}{\pi} \{ G_a + G_b + G_e \} \right] \quad (2.17) \end{aligned}$$

where G_a, G_b, G_c, G_d and G_e are functions of the ratio m_c/m_b , and are obtained by adding the contributions of particular diagrams, which we label by Roman numbers:

$$\frac{\alpha_s}{\pi} G_a = K \text{Im} (\text{II} + \text{II}^\dagger + \text{III} + \text{IX} + \text{IX}^\dagger + \text{XII}),$$

$$\frac{\alpha_s}{\pi} G_b = K \text{Im} (\text{IV} + \text{V} + \text{VII}),$$

$$\begin{aligned}
\frac{\alpha_s}{\pi} G_c &= K \operatorname{Im} (\text{II} + \text{II}^\dagger + \text{V} + \text{XI} + \text{XI}^\dagger + \text{XII}), \\
\frac{\alpha_s}{\pi} G_d &= K \operatorname{Im} (\text{III} + \text{IV} + \text{VI}), \\
\frac{\alpha_s}{\pi} G_e &= K \operatorname{Im} (\text{VI} + \text{VIII} + \text{X} + \text{X}^\dagger + \text{XI} + \text{XI}^\dagger).
\end{aligned} \tag{2.18}$$

Here

$$K = \frac{192\pi^3}{m_b^6 f_1(m_c^2/m_b^2)}. \tag{2.19}$$

Note that the colour-factors are split off and shown explicitly in (2.17).

It is easy to verify that G_a and G_b are manifestly gauge-invariant and do not depend on the scheme used for γ_5 . The same is true for G_c and G_d provided the renormalization scheme preserves Fierz-symmetry (cf. the next subsection). Taking into account the relation (2.9), the contribution of matching coefficients in the second line in (2.17) can equivalently be rewritten replacing G_e in the last line by $G_e + B$, which is again a scheme-independent quantity.

The reason for splitting the full radiative correction to the nonleptonic inclusive width into several pieces is that some of these expressions also appear in the semileptonic decay widths. For example, the $b \rightarrow ce\bar{\nu}$ decay rate can be written in terms of the function G_a as

$$\Gamma(b \rightarrow ce\bar{\nu}) = \Gamma_0 \left\{ 1 + \frac{2}{3} \frac{\alpha_s(\mu)}{\pi} G_a \right\} \tag{2.20}$$

and, owing to Fierz-identities, the function G_c determines the radiative corrections to the decay $b \rightarrow u\tau\bar{\nu}$,

$$\Gamma(b \rightarrow u\tau\bar{\nu}) = \Gamma_0 \left\{ 1 + \frac{2}{3} \frac{\alpha_s(\mu)}{\pi} G_c \right\}, \tag{2.21}$$

with the obvious replacements $V_{cb} \rightarrow V_{ub}$ and $a = (m_c/m_b)^2 \rightarrow (m_\tau/m_b)^2$ in Γ_0 and G_c . Since the radiative correction to the semileptonic decay $b \rightarrow ce\bar{\nu}$ is known analytically for arbitrary c quark mass, we can incorporate the answer given in [8] directly in the expression for the nonleptonic width and do not need to calculate the function G_a anew.

Finally, the calculation of G_b and G_d is simplified by using the known results for the radiative correction to the vector correlation function with one massive quark:

$$\begin{aligned}
\Pi_{\mu\nu} &= i \int d^4x e^{iqx} \langle 0 | T[\bar{q}\gamma_\mu Q(x) \bar{Q}\gamma_\nu q(0)] | 0 \rangle \\
&= \int_{m_c^2}^{\infty} \frac{ds}{s - q^2} \left\{ q_\mu q_\nu \rho_1^V(s) + g_{\mu\nu} \rho_2^V(s) \right\} + \text{constants}.
\end{aligned} \tag{2.22}$$

The expressions for the spectral densities $\rho_i^V(s)$ can be obtained from [19]; we have also calculated them directly using Cutkosky rules (cf. App. C). Thus, essentially only G_c and G_e remain to be calculated, i.e. the diagrams II, V, VI, VIII, X, XI and XII.

It is worthwhile to note that the expressions for G_a and G_b are available in form of one-dimensional parametric integrals for arbitrary masses of all the three final state quarks from [7]², corresponding to the upper and lower vertex corrections, respectively, in the notation of this paper. Answers for G_c and G_d can be inferred from the expressions given in [7] by Fierz-transformations. However, the calculation of G_e involves different Feynman diagrams than those calculated in [7] and is new.

2.3 Calculational Tools

In this paper we use the well-known dispersion technique and calculate the imaginary parts of the necessary diagrams by explicitly summing the contributions of different discontinuities, corresponding to real gluon emission and virtual corrections. Infra-red (IR) divergences, which are bound to arise due to the presence of massless particles in the final state, are regulated by introducing non-zero gluon and light quark masses. According to the famous Bloch–Nordsieck theorem, all IR divergences cancel in the sum of all possible discontinuities for a given diagram, so that in the final answer for the total imaginary part one can put the regulator masses to zero. In principle, one could escape the problem with the IR divergences altogether calculating the matrix element in question in Euclidian space, continuing analytically to Minkowski space and taking the imaginary part. This technique is very powerful for massless quarks, but, as we have found, is not very useful when quark masses have to be taken into account. As for diagram V, we prefer to express the subdiagram containing the self-energy by a regularized dispersion relation and only then compute the discontinuity.

We further use dimensional regularization and the $\overline{\text{MS}}$ subtraction scheme to deal with ultraviolet divergences, which give rise to the renormalization of operators and quark masses.

Due to the presence of γ_5 , the use of dimensional regularization involves subtleties that have received a lot of attention over the last years. We have found that for our purposes it is sufficient to use the simplest prescription with anticommuting γ_5 in D dimensions, NDR. It is known that this scheme can yield algebraic inconsistencies when the amplitude in question contains closed fermion loops. Our method of calculation explicitly avoids computing such diagrams by the appropriate use of Fierz-symmetry. Indeed, by applying Fierz-transformations one can always achieve that any diagram contains no dangerous closed fermion loops,³ as illustrated in Fig. 2. Subtleties are bound to arise, however, if the Fierz-symmetry is broken by regularization. Thus, we use the results of Buras and Weisz [16] who have checked that in the NDR scheme the renormalized operators \mathcal{O}_1 and

²We use the expressions given in the second of Refs. [7] and imply that the factors $\ln \Delta/w$ appearing in Eq. (3.35) of this paper should be understood as $(\ln \Delta)/w$, as we have found by comparison to the first of Refs. [7], and to the numerical results given in [7].

³In fact, closed fermion loops with only one external momentum and at most two open Lorentz-indices do not pose a problem, since $\text{Tr}(\gamma_\mu \gamma_\nu \gamma_5)$ vanishes in any dimension.

\mathcal{O}_2 have the same properties under Fierz-transformations as the bare ones,

$$\mathcal{O}_2 \xrightarrow{\text{Fierz}} \mathcal{O}_1 (c \leftrightarrow d), \quad \mathcal{O}_1 \xrightarrow{\text{Fierz}} \mathcal{O}_2 (c \leftrightarrow d). \quad (2.23)$$

Furthermore, with the particular choice of evanescent operators made in [16] this property is valid *diagram by diagram*: after subtraction of counterterms, renormalized Feynman diagrams that can be related to each other by means of Fierz-transformations in four dimensions coincide identically. Note that we are only interested in the imaginary parts of the multi-loop diagrams of Fig. 1, which are given by the product of at most one-loop and tree-level amplitudes, followed by phase-space integration. Thus, evaluating the product with *renormalized* amplitudes, one can avoid the contributions of evanescent operators altogether, provided their choice is consistent with the calculation of the one-loop matching coefficients B_{\pm} by a naïve projection onto four dimensions, see [16] for details. We have checked that the alternative procedure for calculating the whole three-loop diagram in dimension D , taking into account the counterterms due to the evanescent operators as given in [16], yields the same result. Last but not least, we have found that in the limit $m_c \rightarrow 0$, our answers coincide with those obtained by Altarelli et al., [5], using dimensional reduction, and by Buchalla, [6], using the 't Hooft-Veltman scheme, cf. App. B.8. More details about the calculation and some useful intermediate formulas can be found in appendices A to C.

3 Analytic results

In this section we give the explicit expressions for the next-to-leading order corrections to the nonleptonic rate $b \rightarrow c\bar{u}d$, the functions G_x defined in Eq. (2.18). The answers for all necessary single diagrams are given in App. B. Throughout this section, we use $a = (m_c/m_b)^2$; the factor K was defined in (2.19) and the phase-space function f_1 in (2.15). All results are given in terms of pole masses.

As mentioned before, G_a is proportional to the semileptonic width $\Gamma(b \rightarrow ce\bar{\nu})$. From the analytical result given in [8] we obtain:

$$\begin{aligned} \frac{1}{K} \frac{\alpha_s}{\pi} G_a = & -\frac{g_s^2 m_b^6}{9216\pi^5} \left\{ -(1-a^2)(75-956a+75a^2) + 4(1-a^2) \right. \\ & \times (17-64a+17a^2) \ln(1-a) + 4a(60+270a-4a^2+17a^3) \ln a \\ & - 48(1+30a^2+a^4) \ln a \ln(1-a) + 12a^2(36+a^2) \ln^2 a \\ & - 384a^{3/2}(1+a) \left[\pi^2 - 2 \ln \frac{1-a^{1/2}}{1+a^{1/2}} \ln a + 4\text{L}_2(-a^{1/2}) - 4\text{L}_2(a^{1/2}) \right] \\ & \left. - 12(1+16a^2+a^4)(-\pi^2+6\text{L}_2(a)) \right\}. \end{aligned} \quad (3.1)$$

We next calculate G_b and G_d by exploiting the result for the vector correlation function given in [19]. To get G_d , we first apply a Fierz-transformation to both four-quark vertices of the diagrams III, IV and VI, cf. Fig. 2. We then express the closed fermion loops by twice the radiative corrections to the vector correlation function⁴ $\Pi_{\mu\nu}$ defined in Eq. (2.22) in their dispersion representation. This effectively replaces the loop by the propagator of a pseudoparticle, whose mass is just the invariant mass of the original two fermions, multiplied by the weight functions $\rho_i^{(2)}$ given in App. C and followed by integration over phase-space. By cutting the two remaining propagator lines we obtain the sum of imaginary parts of the diagrams III + IV + VI:

$$\frac{1}{K} \frac{\alpha_s}{\pi} G_d = \frac{1}{4\pi m_b^2} \int_{m_c^2}^{m_b^2} ds (m_b^2 - s)^2 \left[m_b^2 \rho_1^{(2)}(s) - 2\rho_2^{(2)}(s) \right]. \quad (3.2)$$

The integral can easily be done with the formulas given in App. A. The final result is:

$$\begin{aligned} \frac{1}{K} \frac{\alpha_s}{\pi} G_d = & \frac{g_s^2 m_b^6}{9216\pi^5} \left\{ (1-a)(18 - 476a - 539a^2 + 75a^3) \right. \\ & + 4a^2(36 + 8a - a^2) (\pi^2 - 3 \ln^2 a) \\ & - 2(1-a^2) \left[31 - 320a + 31a^2 - 12(1-8a+a^2) \ln a \right] \ln(1-a) \\ & - 2a(132 + 90a - 308a^2 + 31a^3) \ln a \\ & + 24(2 - 16a - 36a^2 + 8a^3 - a^4 + 12a^2 \ln a) L_2(a) \\ & \left. + 864a^2 [\zeta(3) - L_3(a)] \right\}. \end{aligned} \quad (3.3)$$

For G_b , the fermions in the loop are massless, so that

$$\begin{aligned} \frac{1}{K} \frac{\alpha_s}{\pi} G_b = & \frac{1}{4\pi m_b^2} \int_0^{(m_b-m_c)^2} ds \left\{ \left[(m_b^2 - m_c^2)^2 - (m_b^2 + m_c^2)s \right] \rho_1^{(2)}(s) \Big|_{\text{massless}} \right. \\ & \left. - 2(m_b^2 + m_c^2 - s) \rho_2^{(2)}(s) \Big|_{\text{massless}} \right\} w(s, m_b^2, m_c^2) \\ = & \frac{g_s^2 m_b^6}{512\pi^5} f_1(a), \end{aligned} \quad (3.4)$$

where w is defined as

$$w(x, y, z) = (x^2 + y^2 + z^2 - 2xy - 2xz - 2yz)^{1/2}. \quad (3.5)$$

Since K is proportional to $1/f_1(a)$, the above result simply means that G_b is a constant independent of a .

⁴Note that the vector correlation function equals the axial vector correlation function in perturbative QCD.

Summing up the diagrams II, II[†], V, XI, XI[†] and XII one gets

$$\begin{aligned}
\frac{1}{K} \frac{\alpha_s}{\pi} G_c = & \frac{g_s^2 m_b^6}{9216 \pi^5} \left\{ (1-a)(75 - 539a - 476a^2 + 18a^3) \right. \\
& - 4(3 - 24a - 36a^2 + 16a^3 - 2a^4) \pi^2 \\
& - 2(1-a^2) \left[31 - 320a + 31a^2 + 12(1-8a+a^2) \ln a \right] \ln(1-a) \\
& - 2a(12 + 90a - 188a^2 + 31a^3 - 48a\pi^2) \ln a \\
& - 24(1-8a + 36a^2 + 16a^3 - 2a^4 + 12a^2 \ln a) L_2(a) \\
& \left. + 864a^2 [L_3(a) - \zeta(3)] \right\}. \tag{3.6}
\end{aligned}$$

Finally, summing up the diagrams VI, VIII, X, X[†], XI, XI[†], we obtain the scheme-independent quantity $G_e + B$:

$$\begin{aligned}
\frac{1}{K} \frac{\alpha_s}{\pi} (G_e + B) = & \frac{g_s^2 m_b^6}{1536 \pi^5} \left\{ -(1-a^2)(41 - 488a + 41a^2) - 16a(1+3a+a^2)[\pi^2 - 6L_2(a)] \right. \\
& - 8(1-a^2)(1+28a+a^2) \ln(1-a) + 4a^2(120 - 32a - 5a^2) \ln a \\
& \left. + 48a^3 \ln^2 a + 2(6 \ln(m_b^2/\mu^2) + 11) f_1(a) \right\}. \tag{3.7}
\end{aligned}$$

Note that G_e contains a logarithm of μ , namely $G_e = 6 \ln(m_b^2/\mu^2) + \dots$, which just cancels the remaining μ dependence of the leading order term in Eq. (2.17), as shown by an explicit expansion around $\mu = m_b$:

$$2L_+^2(\mu) + L_-^2(\mu) = 2L_+^2(m_b) + L_-^2(m_b) - \frac{1}{2} \left\{ L_+^2(m_b) - L_-^2(m_b) \right\} \frac{2}{3} \frac{\alpha_s(m_b)}{\pi} 6 \ln \frac{m_b^2}{\mu^2}. \tag{3.8}$$

This completes the list of entries required to evaluate the radiative corrections to the nonleptonic decay $b \rightarrow c \bar{u} d$. We have checked that our expressions for G_c and G_d agree numerically to the results given in [7]. As mentioned above, the answer for G_e cannot be inferred from this paper.

For practical calculations, it may be useful to give approximations to the above formulas for small a :

$$\begin{aligned}
(G_a + G_b) f_1(a) = & \frac{31}{4} - \pi^2 - a[80 + 24 \ln a] + 32a^{3/2} \pi^2 - a^2[273 + 16\pi^2 - 18 \ln a \\
& + 36 \ln^2 a] + 32a^{5/2} \pi^2 - \frac{8}{9} a^3 [118 - 57 \ln a] + \mathcal{O}(a^{7/2}), \tag{3.9}
\end{aligned}$$

$$(G_c + G_d) f_1(a) = \frac{31}{4} - \pi^2 - 8a[10 - \pi^2 + 3 \ln a] - a^2[117 - 24\pi^2$$

$$\begin{aligned}
& + (30 - 8\pi^2) \ln a + 36 \ln^2 a] - \frac{4}{3} a^3 [79 + 2\pi^2 \\
& - 62 \ln a + 6 \ln^2 a] + \mathcal{O}(a^4), \tag{3.10}
\end{aligned}$$

$$\begin{aligned}
(G_a + G_b + G_e + B)f_1(a) &= \left(6 \ln \frac{m_b^2}{\mu^2} + 11\right) f_1(a) - \frac{51}{4} - \pi^2 + 8a[21 - \pi^2 - 3 \ln a] \\
& + 32a^{3/2} \pi^2 - a^2[111 + 40\pi^2 - 258 \ln a + 36 \ln^2 a] \\
& + 32a^{5/2} \pi^2 - \frac{4}{9} a^3 [305 + 18\pi^2 + 30 \ln a - 54 \ln^2 a] \\
& + \mathcal{O}(a^{7/2}). \tag{3.11}
\end{aligned}$$

These approximations are valid for $a < 0.15$, which covers a realistic range of values $(m_c/m_b)^2$.

The corresponding approximate formula for the semileptonic decay $b \rightarrow ce\bar{\nu}$ is given in [8]. We repeat it here for completeness, converting to our notations, cf. (2.20):

$$\begin{aligned}
G_a f_1(a) &= \frac{25}{4} - \pi^2 - a[68 + 24 \ln a] + 32a^{3/2} \pi^2 - a^2[16\pi^2 + 273 - 36 \ln a + 36 \ln^2 a] \\
& + 32a^{5/2} \pi^2 - a^3 \left[\frac{1052}{9} - \frac{152}{3} \ln a \right] + \mathcal{O}(a^{7/2}). \tag{3.12}
\end{aligned}$$

Similarly, we obtain for $b \rightarrow u\tau\bar{\nu}$, cf. (2.21):

$$\begin{aligned}
G_c f_1(a) &= \frac{25}{4} - \pi^2 - 8a[6 - \pi^2] - 2a^2[15 - 6\pi^2 + (15 - 4\pi^2) \ln a + 36\zeta(3)] \\
& + a^3 \left[20 - \frac{16\pi^2}{3} \right] + \mathcal{O}(a^4), \tag{3.13}
\end{aligned}$$

where here a has to be interpreted as $(m_\tau/m_b)^2$.

These expressions complete our formulas of radiative corrections to b quark decays with one massive particle in the final state.

4 Estimate of Finite Mass Corrections to $\Gamma(b \rightarrow c\bar{c}s)$

The structure of the decay rate $\Gamma(b \rightarrow c\bar{c}s)$ is very similar to $\Gamma(b \rightarrow c\bar{u}d)$, except for the additional contributions of penguin diagrams. Since penguin operators enter the effective Lagrangian only by mixing, their Wilson-coefficients are small and thus penguin contributions can usually be neglected in tree-level decays, cf. [11]. Defining functions H_x in a

completely analogous way to the G_x that enter $\Gamma(b \rightarrow c\bar{u}d)$, Eq. (2.17), the decay rate of $b \rightarrow c\bar{c}s + c\bar{c}d$ can be written as

$$\begin{aligned} \Gamma(b \rightarrow c\bar{c}s + c\bar{c}d) = & \Gamma'_0 \left[2L_+^2(\mu) + L_-^2(\mu) + \frac{\alpha_s(m_W) - \alpha_s(\mu)}{2\pi} \{2L_+^2(\mu)R_+ + L_-^2(\mu)R_-\} \right. \\ & + \frac{\alpha_s(\mu)}{2\pi} \{2L_+^2(\mu)B_+ + L_-^2(\mu)B_-\} \\ & + \frac{3}{4} \{L_+(\mu) + L_-(\mu)\}^2 \frac{2}{3} \frac{\alpha_s(\mu)}{\pi} \{H_a + H_b\} \\ & + \frac{3}{4} \{L_+(\mu) - L_-(\mu)\}^2 \frac{2}{3} \frac{\alpha_s(\mu)}{\pi} \{H_c + H_d\} \\ & \left. + \frac{1}{2} \{L_+^2(\mu) - L_-^2(\mu)\} \frac{2}{3} \frac{\alpha_s(\mu)}{\pi} \{H_a + H_b + H_e\} \right] + \text{penguins}. \end{aligned} \quad (4.1)$$

The tree-level decay rate Γ'_0 is defined as in Eq. (2.14) except for the phase-space factor. Neglecting the strange quark mass, $f_1(a)$ has to be replaced by

$$f_1(a, a) = \sqrt{1-4a} \left(1 - 14a - 2a^2 - 12a^3 \right) + 24a^2 \left(1 - a^2 \right) \ln \left(\frac{1 + \sqrt{1-4a}}{1 - \sqrt{1-4a}} \right) \quad (4.2)$$

with $a = (m_c/m_b)^2$. With $m_s = 0.2 \text{ GeV}$, (4.2) is accurate to better than 5% for $a < 0.35^2$. In the subsequent estimate of $\Gamma(b \rightarrow c\bar{c}s)$, however, we take into account a finite m_s and use the three-particle phase-space factors calculated in [20].

H_a parametrizes the corrections to the decay rate $b \rightarrow c\tau\bar{\nu}$ with the “ τ ” and the c quark degenerate in mass, whereas H_c now describes the corrections to a decay of type $b \rightarrow u\tau\bar{\nu}$, where the light quark u is still massless, but the *leptons* have equal *finite* masses.

The calculation of H_b requires only expressions already obtained in this paper. From Eq. (3.4), where G_b is expressed as a single integral over spectral functions, we immediately obtain:

$$\begin{aligned} \frac{1}{K'} \frac{\alpha_s}{\pi} H_b = & \frac{1}{4\pi m_b^2} \int_{m_c^2}^{(m_b-m_c)^2} ds \left\{ [(m_b^2 - m_c^2)^2 - (m_b^2 + m_c^2)s] \rho_1^{(2)}(s) \right. \\ & \left. - 2(m_b^2 + m_c^2 - s) \rho_2^{(2)}(s) \right\} w(s, m_b^2, m_c^2) \end{aligned} \quad (4.3)$$

with w defined in (3.5) and $\rho_i^{(2)}$ given in App. C. K' equals K , Eq. (2.19), except for the obvious replacement of phase-space factors, $f_1(a) \rightarrow f_1(a, a)$. H_b is extremely sensitive to the value of the c quark mass as clearly visible from Tab. 2; recall that the corresponding quantity for $b \rightarrow c\bar{u}d$, G_b , was constant in m_c ! The numerical values given in Tab. 2 agree with the corresponding ones obtainable from [7]. In the table we also give the values of H_a , H_c and H_d as functions of m_c/m_b calculated from the formulas in [7]. H_e cannot be obtained

from the work of Hokim and Pham, so for the present estimate we insert $H_e \approx G_e$, Eq. (3.7), and estimate the error introduced by this procedure by twice the difference between $G_e(a)$ and $G_e(0)$. From Tab. 2 it is clear that both $H_a + H_b$ and $H_c + H_d$ are extremely sensitive to m_c . For the realistic value $m_c/m_b \approx 0.3$, both $H_a + H_b$ and $H_c + H_d$ are positive and by a factor four to five larger than the corresponding G_x . In Tab. 3 we also give the decay rate $\Gamma(b \rightarrow c\bar{c}s)$ including the error in H_e . For $m_c/m_b = 0.3$, the finite c quark mass effects in the radiative corrections increase the decay rate by 30%.

5 Numerical Results

Let us now turn to the numerical analysis of the results obtained in Secs. 3 and 4. To do this, we first rewrite the decay width Eq. (2.17) in a form that is more convenient in the present context ($a = (m_c/m_b)^2$). Introducing scheme-independent coefficients c_{ij} by $c_{11} = G_c + G_d$, $c_{12} = G_a + G_b + G_e + B$ and $c_{22} = G_a + G_b$, we have

$$\begin{aligned} \Gamma(b \rightarrow c\bar{u}d + c\bar{u}s) = \Gamma_0 \left[2L_+^2(\mu) + L_-^2(\mu) + \frac{\alpha_s(m_W) - \alpha_s(\mu)}{2\pi} \{2L_+^2(\mu)R_+ + L_-^2(\mu)R_-\} \right. \\ \left. + \frac{3}{4} \{L_+(\mu) + L_-(\mu)\}^2 \frac{2}{3} \frac{\alpha_s(\mu)}{\pi} c_{22}(a) + \frac{3}{4} \{L_+(\mu) - L_-(\mu)\}^2 \frac{2}{3} \frac{\alpha_s(\mu)}{\pi} c_{11}(a) \right. \\ \left. + \frac{1}{2} \{L_+^2(\mu) - L_-^2(\mu)\} \frac{2}{3} \frac{\alpha_s(\mu)}{\pi} c_{12}(a) \right] \end{aligned} \quad (5.1)$$

$$\equiv 3\Gamma_0 \eta(\mu) J(a, \mu). \quad (5.2)$$

Here we use the same notations as [11] with

$$\eta(\mu) = \frac{1}{3} \{2L_+^2(\mu) + L_-^2(\mu)\}, \quad (5.3)$$

whereas $J = 1 + \mathcal{O}(\alpha_s)$ covers the next-to-leading order terms.

In Fig. 3, the coefficients c_{11} , $c_{12}(\mu = m_b)$ and c_{22} are plotted as functions of m_c/m_b ; we have also tabulated the numerical values in Tab. 4. A range of realistic values of m_c/m_b , $0.26 \leq m_c/m_b \leq 0.32$, is indicated by a grey bar. The figure shows clearly that the colour-favoured coefficient c_{22} is not very sensitive to the c quark mass. This is due to the fact that $G_b \equiv 3/2$ is constant in m_c , whereas the term G_a , which also determines the semileptonic decay width, exhibits an only mild dependence on m_c . The coefficient c_{12} increases more steeply in m_c , but is suppressed in the rate by a small Wilson-coefficient. Both c_{12} and c_{22} are finite for $m_c \rightarrow m_b$. This is different for c_{11} : this function diverges like $\sim \ln(m_b - m_c)$ as shown in Tab. 4. Note, however, that the decay rate still vanishes for $m_c = m_b$. For c_{11} and c_{22} we found agreement with the integrals given in [7].

We next investigate the behaviour of $\Gamma(b \rightarrow c\bar{u}d)$ as compared to $\Gamma(b \rightarrow ce\bar{\nu})$. To this purpose, we introduce

$$I(a, \mu) = 1 + \frac{2}{3} \frac{\alpha_s(\mu)}{\pi} G_a(a), \quad (5.4)$$

so that $\Gamma(b \rightarrow ce\bar{\nu}) = \Gamma_0 I(a, \mu)$. In Fig. 4(a) we plot $I(a, \mu)/I(0, \mu)$ as function of m_c/m_b for three different values of the renormalization scale μ . Fig. 4(b) shows the ratio $J(a, \mu)/J(0, \mu)$ as function of m_c/m_b . For $m_c/m_b \approx 0.3$, we find an increase of the nonleptonic decay rate $b \rightarrow c\bar{u}d$ by (4–8)%, depending on the renormalization scale. Comparing the two plots, we find that in the range of realistic values of m_c/m_b , which is emphasized by a grey bar, the enhancement by finite mass corrections is approximately equal for semi- and nonleptonic decays, whereas for m_c/m_b near one, the logarithmic divergence in c_{11} clearly dominates.

Whereas up to now we have discussed only quantities that are defined on a purely partonic level, one clearly is more interested in predictions of *hadronic* decay rates and branching ratios. Though in general this requires the knowledge of hadronic matrix elements, matters simplify considerably for inclusive decays of heavy hadrons. Without going into further details, we just mention that the theory of inclusive decays of heavy hadrons has experienced considerable progress over the last years when another field of application of the well-known operator product expansion (OPE) technique as an expansion in inverse powers of the heavy quark mass was opened, see [1, 2]. The situation is even more favourable than in other fields since the leading term in the heavy quark expansion does not involve *any* hadronic uncertainties, but simply coincides with the underlying free quark decay process. Hadronic corrections enter only at second and higher order in the expansion with a natural size of $\sim 1 \text{ GeV}^2/m_b^2 \sim 5\%$.

To second order in the heavy quark expansion, these corrections can be expressed in terms of two matrix elements,

$$\begin{aligned} 2m_B\lambda_1 &= \langle B | \bar{b}_v (iD)^2 b_v | B \rangle, \\ 6m_B\lambda_2 &= \langle B | \bar{b}_v \frac{g}{2} \sigma_{\mu\nu} F^{\mu\nu} b_v | B \rangle, \end{aligned} \quad (5.5)$$

where b_v is defined as $b_v = e^{im_b v x} b(x)$, $b(x)$ being the b quark field in full QCD, v_μ is the four-velocity of the B meson, m_B its mass and $F^{\mu\nu}$ the gluonic field-strength tensor.

Whereas λ_2 is directly related to the observable spectrum of beautiful mesons,

$$\lambda_2 \approx \frac{1}{4} (m_{B^*}^2 - m_B^2) = 0.12 \text{ GeV}^2, \quad (5.6)$$

the quantity λ_1 is difficult to measure, cf. [21]. Physically, $-\lambda_1/(2m_b)$ is just the average kinetic energy of the b quark inside the meson. At present, only a QCD sum rule estimate is available, according to which $\lambda_1 \simeq -0.6 \text{ GeV}^2$ [22]. This result has been met with caution (see, e.g. [23]), since it corresponds in fact to a surprisingly large momentum of the b quark inside the meson of order (700–800) MeV. However, in a recent series of papers, cf. [21, 24], an upper bound on λ_1 has been derived, to wit $\lambda_1 \leq -0.4 \text{ GeV}^2$, which appears to be in nice agreement with the QCD sum rule prediction. In our analysis we thus conform to the value $\lambda_1 = -(0.6 \pm 0.1) \text{ GeV}^2$.

Taking into account hadronic corrections, the nonleptonic decay rate of a B meson into

a single charmed hadronic state can be written as [2]:

$$\Gamma(B \rightarrow X_c) = 3\Gamma_0 \left[\eta(\mu) J(a, \mu) \left\{ 1 + \frac{\lambda_1}{2m_b^2} + \frac{3\lambda_2}{2m_b^2} - \frac{6(1-a)^4}{f_1(a)} \frac{\lambda_2}{m_b^2} \right\} - \left\{ L_+^2(\mu) - L_-^2(\mu) \right\} \frac{4(1-a)^3}{f_1(a)} \frac{\lambda_2}{m_b^2} + \mathcal{O}\left(\alpha_s^2, \frac{\alpha_s}{m_b^2}, \frac{1}{m_b^3}\right) \right]. \quad (5.7)$$

For the semileptonic rate one obtains:

$$\Gamma(B \rightarrow X_c e \bar{\nu}) = \Gamma_0 \left[I(a, \mu) \left\{ 1 + \frac{\lambda_1}{2m_b^2} + \frac{3\lambda_2}{2m_b^2} - \frac{6(1-a)^4}{f_1(a)} \frac{\lambda_2}{m_b^2} \right\} + \mathcal{O}\left(\alpha_s^2, \frac{\alpha_s}{m_b^2}, \frac{1}{m_b^3}\right) \right]. \quad (5.8)$$

In evaluating these decay rates, it is crucial to minimize the number of independent parameters. In doing so, we take advantage of the fact that the *difference* between heavy quark masses is fixed in the framework of the heavy quark expansion:

$$m_b - m_c = m_B - m_D + \frac{\lambda_1 + 3\lambda_2}{2} \left(\frac{1}{m_b} - \frac{1}{m_c} \right) + \mathcal{O}\left(\frac{1}{m^2}\right). \quad (5.9)$$

The only quantity remaining to be fixed is then m_b or m_c . We prefer to take m_b from spectroscopy and choose the most conservative range⁵

$$4.5 \text{ GeV} \leq m_b \leq 5.1 \text{ GeV}. \quad (5.10)$$

With these values we find:

$$\frac{\Gamma(B \rightarrow X_c)}{\Gamma(B \rightarrow X_c e \bar{\nu})} = 4.0 \pm 0.4. \quad (5.11)$$

This result is nearly independent of the c quark mass; the error is entirely due to the dependence on the renormalization scale, $m_b/2 \leq \mu \leq 2m_b$. Note that it is mainly the mass-independent G_b that enters the radiative corrections, whereas G_a cancels, which explains the small sensitivity of (5.11) to m_c .

Finally we calculate the semileptonic branching ratio as

$$B(B \rightarrow X e \bar{\nu}) = \frac{\Gamma(B \rightarrow X e \bar{\nu})}{\sum_{\ell=e, \mu, \tau} \Gamma(B \rightarrow X \ell \bar{\nu}_\ell) + \Gamma(B \rightarrow X_c) + \Gamma(B \rightarrow X_c \bar{c})}. \quad (5.12)$$

Previous analyses yielded $B(B \rightarrow X e \bar{\nu}) > 12.5\%$ [11, 13] which is considerably bigger than what is measured experimentally, $B(B \rightarrow X e \bar{\nu}) = (10.43 \pm 0.24)\%$ [26]. Yet these studies were lacking the finite quark mass effects on $J(a, \mu)$, the radiative corrections to $\Gamma(b \rightarrow c \bar{c} s)$ and the corrections to $\Gamma(b \rightarrow c \tau \bar{\nu})$. Taking them into account, we find $B(B \rightarrow X e \bar{\nu}) = (11.6 \pm 1.8)\%$ where the error comes from the uncertainty in the renormalization scale, in

⁵Since we give a broad range of values, we are not concerned with the intrinsic uncertainty in the definition of the pole mass which is caused by renormalons and estimated to be of order (50–200) MeV, [25].

λ_1 , in the quark mass and in the value of $\alpha_s(m_Z)$, where we used $\alpha_s(m_Z) = (0.117 \pm 0.007)$ [27]. The functional dependence of the semileptonic branching ratio on m_b with m_c fixed by (5.9) is also plotted in Fig. 5. Note that in $\Gamma(B \rightarrow X_{c\bar{c}})$ in Eq. (5.12) we use the full tree-level phase-space factor calculated in [20] including a strange quark mass $m_s = 0.2 \text{ GeV}$. With that value of m_s , the rate is decreased by typically 5%, which is a much smaller effect than taking into account the c quark mass in the radiative corrections.

In Tab. 5 we compare the semileptonic branching ratios obtained in [11, 13] with ours, using the same input parameters. It turns out that, although the introduction of the heavy quark expansion by Bigi et al. leads to a reduction of the branching ratio by 0.3% compared to the quark level analysis of Altarelli and Petrarca, the finite c quark mass effects in the radiative corrections to the nonleptonic widths are by more than a factor three bigger and yield an additional 1.0% reduction. This fact shows the paramount importance of *perturbative* corrections in the heavy quark expansion.

Yet, we consider this analysis as a rather preliminary one. To make more definite predictions, one has to reduce the scheme-dependence. We plan to come back to this and related questions in a separate publication [28].

6 Summary and Conclusions

In this paper we have calculated the radiative corrections to the free quark decay $b \rightarrow c\bar{u}d$ as the imaginary part of the relevant forward-scattering amplitude including the full dependence on the c quark mass. We have performed the calculation in naïve dimensional regularization (NDR) with anticommuting γ_5 . The key-observation that allowed us to employ this scheme despite of its known deficiencies was that diagrams that are ambiguous in NDR can be related to well-defined ones by means of Fierz-transformations. In the limit $m_c \rightarrow 0$, our results agree with known expressions obtained in other schemes. As far as comparison is possible, our results also agree with those of [7].

For realistic values of the b and the c quark mass, we find a moderate increase of about (4-8)% of the decay rate $\Gamma(b \rightarrow c\bar{u}d)$ with respect to the limit of vanishing c quark mass, depending on the renormalization scale.

We also have estimated the increase of $\Gamma(b \rightarrow c\bar{c}s)$ by finite mass effects to be about 30%. The calculation of the full radiative corrections is under study.

In the framework of the heavy quark expansion of inclusive decays of heavy hadrons, the knowledge of finite quark mass corrections to nonleptonic decays is crucial for an improvement of the theoretical prediction of various measurable quantities like $\Gamma(B \rightarrow X_c)/\Gamma(B \rightarrow X_c e \bar{\nu})$ and $B(B \rightarrow X e \bar{\nu})$. We have shown that the ratio of non- to semileptonic decays of B mesons to single charmed final states remains nearly unaffected by finite mass effects, whereas the semileptonic branching ratio is reduced by 1.0% compared with a recent investigation by Bigi et al., [13]. The finite mass terms in the radiative corrections are thus of the same importance as the hadronic corrections introduced in [1, 2] and severely reduce the scope of possible new physics in nonleptonic B decays. Yet, the analysis of the semileptonic branching ratio involves delicate points like the choice of quark masses and

estimates of higher order radiative corrections; we will address these points in a separate paper [28].

Acknowledgements

P. B. and V. B. would like to thank B. Stech for bringing the problem to their attention. P. B. is grateful to A. Buras, S. Herrlich, M. Lautenbacher, M. Misiak and U. Nierste for discussions about evanescent operators and related topics. V. B. gratefully acknowledges correspondence with X.Y. Pham concerning Ref. [7]. P. B. and V. B. especially thank the Grup de Física Teòrica of the Universitat Autònoma de Barcelona for the warm hospitality extended to them during their stay there where part of this work has been done. E. B. would like to thank BNL's Theory Group for its hospitality and acknowledges the financial support of the CYCIT, project No. AEN93-0520. P. G. acknowledges gratefully a grant from the Generalitat de Catalunya.

Appendix A

In this appendix we collect some intermediate formulas which can be useful in reproducing our results and related calculations.

A.1 One-Loop Integrals

We define the relevant one-loop integrals as

$$(K, K_\rho, K_{\rho\sigma}) = \int \frac{d^D k}{(2\pi)^D} \frac{(1, k_\rho, k_\rho k_\sigma)}{[(k - p_1)^2 - M^2][(k + p_2)^2 - \mu^2][k^2 - \lambda^2]}, \quad (\text{A.1})$$

where D is the space-time dimension. Throughout the appendixes, it is always assumed that $p_1^2 = M^2 \gg p_2^2 = \mu^2 \gg \lambda^2$. M (μ) plays the rôle of the b or c (u or d) quark mass, whereas λ is the gluon mass which along with μ is used to regularize possible IR singularities of the integrals. The renormalization scale appearing in regularized UV divergent integrals is denoted by ν .

The one-loop integrals can be parametrized as

$$K = -\frac{i}{(4\pi)^2} \widetilde{K}(M^2, q^2), \quad q = p_1 + p_2, \quad (\text{A.2})$$

$$K_\rho = -\frac{i}{(4\pi)^2} \left\{ -2B(M^2, q^2)q_\rho - 2\widetilde{B}(M^2, q^2)p_{2\rho} \right\}, \quad (\text{A.3})$$

$$\begin{aligned} K_{\rho\sigma} = & -\frac{i}{(4\pi)^2} \left\{ A(M^2, q^2)q_\rho q_\sigma + B(M^2, q^2)[p_{2\rho}q_\sigma + p_{2\sigma}q_\rho] + \widetilde{B}(M^2, q^2)p_{2\rho}p_{2\sigma} \right. \\ & \left. + C(M^2, q^2)g_{\rho\sigma} \right\} \end{aligned} \quad (\text{A.4})$$

with

$$\begin{aligned}\widetilde{K}(M^2, q^2) = \frac{1}{4(M^2 - q^2)} & \left\{ 2 \ln \frac{\lambda^2}{M^2 - q^2} \left(\ln \frac{\mu^2}{M^2 - q^2} + \ln \frac{M^2}{M^2 - q^2} \right) \right. \\ & \left. - \ln^2 \frac{\mu^2}{M^2 - q^2} - \ln^2 \frac{M^2}{M^2 - q^2} - 4 \text{L}_2 \left(\frac{q^2}{q^2 - M^2} \right) \right\},\end{aligned}\quad (\text{A.5})$$

$$A(M^2, q^2) = \frac{1}{2q^2} \left\{ 1 + \left(1 - \frac{M^2}{q^2} \right) \ln \frac{M^2}{M^2 - q^2} \right\}, \quad (\text{A.6})$$

$$B(M^2, q^2) = -\frac{1}{2q^2} \ln \frac{M^2}{M^2 - q^2}, \quad (\text{A.7})$$

$$\widetilde{B}(M^2, q^2) = -\frac{1}{2(M^2 - q^2)} \left\{ \ln \frac{\mu^2}{M^2 - q^2} + \ln \frac{M^2}{M^2 - q^2} \right\}, \quad (\text{A.8})$$

$$\begin{aligned}C(M^2, q^2) = -\frac{\nu^{D-4}}{4} & \left\{ \frac{2}{4-D} + \ln 4\pi - \gamma_E - \ln \frac{M^2}{\nu^2} \right. \\ & \left. + 3 + \left(1 - \frac{M^2}{q^2} \right) \ln \frac{M^2}{M^2 - q^2} \right\}.\end{aligned}\quad (\text{A.9})$$

Only $C(M^2, q^2)$ is UV divergent. Both $\widetilde{K}(M^2, q^2)$ and $\widetilde{B}(M^2, q^2)$ are IR divergent, while $A(M^2, q^2)$ and $B(M^2, q^2)$ are UV and IR finite.

For $q^2 > M^2$ these functions become complex. It then proves convenient to separate real and imaginary parts explicitly:

$$\begin{aligned}\widetilde{K}(M^2, q^2 > M^2) = \frac{1}{4(M^2 - q^2)} & \left\{ 2 \ln \frac{\lambda^2}{q^2 - M^2} \left(\ln \frac{\mu^2}{q^2 - M^2} + \ln \frac{M^2}{q^2 - M^2} \right) \right. \\ & - \ln^2 \frac{\mu^2}{q^2 - M^2} - \ln^2 \frac{M^2}{q^2 - M^2} + 4 \text{L}_2 \left(\frac{M^2}{M^2 - q^2} \right) \\ & + 4 \ln \frac{q^2}{q^2 - M^2} \ln \frac{M^2}{q^2 - M^2} - \frac{8}{3} \pi^2 \Big\} \\ & + \frac{i\pi}{M^2 - q^2} \left(\ln \frac{\lambda^2}{q^2 - M^2} + \ln \frac{q^2}{q^2 - M^2} \right),\end{aligned}\quad (\text{A.10})$$

$$A(M^2, q^2 > M^2) = \frac{1}{2q^2} \left\{ 1 + \left(1 - \frac{M^2}{q^2} \right) \left(\ln \frac{M^2}{q^2 - M^2} + i\pi \right) \right\}, \quad (\text{A.11})$$

$$B(M^2, q^2 > M^2) = -\frac{1}{2q^2} \left(\ln \frac{M^2}{q^2 - M^2} + i\pi \right), \quad (\text{A.12})$$

$$\tilde{B}(M^2, q^2 > M^2) = -\frac{1}{2(M^2 - q^2)} \left\{ \ln \frac{\mu^2}{q^2 - M^2} + \ln \frac{M^2}{q^2 - M^2} + 2i\pi \right\}, \quad (\text{A.13})$$

$$C(M^2, q^2 > M^2) = -\frac{\nu^{D-4}}{4} \left\{ \frac{2}{4-D} + \ln 4\pi - \gamma_E - \ln \frac{M^2}{\nu^2} \right. \\ \left. + 3 + \left(1 - \frac{M^2}{q^2} \right) \left(\ln \frac{M^2}{q^2 - M^2} + i\pi \right) \right\}. \quad (\text{A.14})$$

A.2 Phase-Space Integrals

Here we collect only the most involved three-particle phase-space integrals. The simpler ones, as well as formulas for n -particle phase-space integrals can be found in [29].

We define

$$\int \text{LIPS}(p_1, p_2, k) \equiv \int \frac{d^3 p_1}{2E_1} \frac{d^3 p_2}{2E_2} \frac{d^3 k}{2E_k} \delta^4(P - p_1 - p_2 - k) \quad (\text{A.15})$$

with $p_2^2 = \mu^2$, $k^2 = \lambda^2$ and keep only logarithms of λ^2 and μ^2 .

$$\int \frac{\text{LIPS}(p_1, p_2, k)}{(\lambda^2 - 2P \cdot k)(\lambda^2 + 2p_2 \cdot k)} = -\frac{\pi^2}{4P^2} \left\{ (P^2 - p_1^2) \tilde{K}(P^2, p_1^2) + E(P^2, p_1^2) \right\}, \quad (\text{A.16})$$

$$\int \frac{\text{LIPS}(p_1, p_2, k)}{\lambda^2 - 2P \cdot k} = -\frac{\pi^2}{4P^2} \left\{ P^2 - p_1^2 - p_1^2 \ln \frac{P^2}{p_1^2} \right\}, \quad (\text{A.17})$$

$$\int \frac{\text{LIPS}(p_1, p_2, k) 2p_2 \cdot k}{\lambda^2 - 2P \cdot k} = -\frac{\pi^2}{16P^2} \left\{ (P^2 - p_1^2)(P^2 + 5p_1^2) - 2p_1^2(p_1^2 + 2P^2) \ln \frac{P^2}{p_1^2} \right\}, \quad (\text{A.18})$$

$$\int \frac{\text{LIPS}(p_1, p_2, k)}{\lambda^2 + 2p_2 \cdot k} = -\frac{\pi^2}{4P^2} \left\{ H(P^2, p_1^2) - 2(P^2 - p_1^2)^2 \tilde{B}(P^2, p_1^2) \right\} \\ = -\frac{\pi^2}{4P^2} \left\{ 2(P^2 - p_1^2)^2 \text{Re } \tilde{B}(p_1^2, P^2) - H(p_1^2, P^2) \right\}, \quad (\text{A.19})$$

$$\int \frac{\text{LIPS}(p_1, p_2, k)}{\lambda^2 + 2p_1 \cdot k} = -\frac{\pi^2}{4P^2} \left\{ P^2 - p_1^2 + P^2 \ln \frac{p_1^2}{P^2} \right\}, \quad (\text{A.20})$$

$$\int \frac{\text{LIPS}(p_1, p_2, k)}{(\lambda^2 + 2p_1 \cdot k)(\lambda^2 + 2p_2 \cdot k)} = -\frac{\pi^2}{4P^2} \left\{ (P^2 - p_1^2) \text{Re } \tilde{K}(p_1^2, P^2) + E'(p_1^2, P^2) \right\}, \quad (\text{A.21})$$

$$\begin{aligned}
\int \text{LIPS}(p_1, p_2, k) \frac{2(p_1 + p_2) \cdot k}{(\lambda^2 + 2p_1 \cdot k)(\lambda^2 + 2p_2 \cdot k)} = \\
= -\frac{\pi^2}{2P^2} \left\{ (P^2 - p_1^2)^2 \text{Re } \tilde{B}(p_1^2, P^2) + P^2 - p_1^2 \right\}. \quad (\text{A.22})
\end{aligned}$$

In addition to the functions defined in the last subsection, we also have used

$$\begin{aligned}
E(x, y) &= \ln \frac{y}{x-y} \ln \frac{x}{x-y} - \frac{\pi^2}{3} + 2 \text{L}_2 \left(\frac{y}{y-x} \right) \\
&= \ln \frac{y}{x} \ln \frac{x}{x-y} - \frac{\pi^2}{3} - 2 \text{L}_2 \left(\frac{y}{x} \right), \quad (\text{A.23})
\end{aligned}$$

$$E'(x, y) = E(y, x) + \frac{\pi^2}{3}, \quad (\text{A.24})$$

$$H(x, y) = x - y + y \ln \frac{x}{y}. \quad (\text{A.25})$$

Note that (A.16), (A.19), (A.21) and (A.22) are IR divergent.

A.3 Integrals Related to Polylogarithms

Our approach yields the relevant diagrams in terms of an integral over the invariant mass squared of two quarks, either both massless or one massive and the other one massless. Using the formulas given in this appendix, the remaining integral can also be done. There appear at most polylogarithms, which are defined as

$$\text{L}_n(y) = \int_0^y \frac{dx}{x} \text{L}_{n-1}(x), \quad \text{L}_0 \equiv -\ln(1-y), \quad (\text{A.26})$$

and have the following simple series expansion in the unit disc:

$$\text{L}_n(y) = \sum_{k=1}^{\infty} \frac{y^k}{k^n}, \quad |y| < 1. \quad (\text{A.27})$$

We need the generic integrals

$$I_n = \int_a^1 dx x^n \ln(1-x) \ln x, \quad (\text{A.28})$$

$$J_n = \int_a^1 dx x^n \text{L}_2(x), \quad (\text{A.29})$$

$$K_n = \int_a^1 dx x^n \ln(x-a) \ln x, \quad (\text{A.30})$$

$$L_n = \int_a^1 dx x^n \text{L}_2 \left(\frac{a}{x} \right) \quad (\text{A.31})$$

for integer n . They can be computed with the help of the following recursion formulas :

$$I_n(n > 0) = \frac{n}{n+1} I_{n-1} + \frac{a^n \ln a}{n+1} \{a + (1-a) \ln(1-a)\} \\ + \frac{1}{n+1} \int_a^1 dx \{x^n + x^{n-1}(1-x) \ln(1-x) + n x^n \ln x\}, \quad (\text{A.32})$$

$$I_0 = 2 - 2a - \frac{\pi^2}{6} - (1-a)(1-\ln a) \ln(1-a) + a \ln a + L_2(a), \quad (\text{A.33})$$

$$I_{-1} = L_2(a) \ln a + \zeta(3) - L_3(a), \quad (\text{A.34})$$

$$I_n(n < -1) = \frac{1}{n+1} \left\{ -a^{n+1} \ln(1-a) \ln a - L_2(1-a) - \frac{1}{2} \ln^2 a \right\} \\ - \frac{1}{n+1} \sum_{k=2}^{-n-1} \frac{1}{(k-1)^2} \left\{ 1 - a^{1-k} [1 + (k-1) \ln a] \right\} \\ - \frac{1}{n+1} \int_a^1 \frac{dx}{x^{-n}} \ln(1-x), \quad (\text{A.35})$$

$$J_n(n \neq -1) = \frac{1}{n+1} \left\{ \frac{\pi^2}{6} - a^{n+1} L_2(a) + \int_a^1 dx x^n \ln(1-x) \right\}, \quad (\text{A.36})$$

$$J_{-1} = \zeta(3) - L_3(a), \quad (\text{A.37})$$

$$K_n = a^{n+1} \int_a^1 \frac{dx}{x^{n+2}} \left\{ \ln^2 \left(\frac{x}{a} \right) + \ln(1-x) \ln a \right\} - a^{n+1} I_{-n-2}, \quad (\text{A.38})$$

$$L_n = a^{n+1} J_{-n-2}. \quad (\text{A.39})$$

Note that the sum in (A.35) evaluates to zero for $n = -2$.

Appendix B

In this appendix we give some details of the computation of the imaginary parts of the diagrams II, V, VI, VIII, X, XI and XII. We have used Cutkosky rules, hence, we think it may be useful for the reader who wishes to reproduce our calculations to give the contributions of the different cuts separately.

Colour-factors are omitted throughout the appendix. In order to get the final answers for the diagrams, one has to multiply by the appropriate colour-factors shown in Tab. 1.

We have used the NDR scheme with anticommuting γ_5 ; for a discussion of this procedure cf. Sec. 2.3. We work in Feynman gauge and use $\overline{\text{MS}}$ subtraction. In contrast to App. A, the renormalization scale is now denoted by μ . The definition of the b quark mass as pole

mass is fixed by the treatment of the diagrams II and XII. The c quark mass is defined by the treatment of the graphs containing the c quark self-energy; we likewise choose the pole mass definition.

Throughout this appendix, we use $a = (m_c/m_b)^2$. The phase-space factor f_1 was defined in (2.15).

B.1 Diagram II

Diagram II is the simplest one. One only needs to multiply the lowest order diagram I by the finite part of the b quark's on-shell wave-function renormalization constant, Z_{2F} :

$$Z_{2F} = \frac{1}{1 - \Sigma'(m_b)} = 1 + C_F \frac{g_s^2}{(4\pi)^2} \left(\frac{2}{D-4} + \gamma_E - \ln 4\pi + \ln \frac{m_b^2}{\mu^2} - 2 \ln \frac{\lambda^2}{m_b^2} - 4 \right), \quad (\text{B.1})$$

where $\Sigma'(m_b)$ is the derivative of the b quark self-energy with respect to \not{p} at $\not{p} = m_b$. The UV divergent piece of Z_{2F} can be subtracted from the imaginary part of diagram II before performing the phase-space integrals. One finally gets (neglecting the colour-factor C_F):

$$\text{Im} [\text{II} + \text{II}^\dagger] = \frac{g_s^2 m_b^2}{1536\pi^5} \left(\ln \frac{m_b^2}{\mu^2} - 2 \ln \frac{\lambda^2}{m_b^2} - 4 \right) f_1(a). \quad (\text{B.2})$$

The IR divergence in the gluon mass, $\ln \lambda^2/m_b^2$, is an artifact of the on-shell normalization and cancels against a corresponding term in Im XII .

B.2 Diagram V

This diagram involves the d quark self-energy. It can be computed in several ways of which we sketch only the simplest one. We first observe that the diagrams IV and V are equal, since the u and the d quark have equal masses, which immediately allows us to write a relation analogous to (3.2) for the twice Fierz-transformed diagram:

$$\text{Im V} = \frac{1}{4\pi m_b^2} \int_{m_c^2}^{m_b^2} ds (m_b^2 - s)^2 \left[m_b^2 \rho_1^{\text{SEL}}(s) - 2\rho_2^{\text{SEL}}(s) \right] \quad (\text{B.3})$$

where the ρ_i^{SEL} are the spectral densities of the light quark's self-energy contribution to the vector correlation function $\Pi_{\mu\nu}$, Eq. (2.22). They are given in Eqs. (C.8) and (C.9). Performing the integral in (B.3) then yields:

$$\begin{aligned} \text{Im V} = \frac{g_s^2 m_b^6}{18432\pi^5} & \left\{ (1 - a^2)(-43 + 296a - 43a^2) - 48a^2 \pi^2 \right. \\ & + 12f_1(a) \left[2 \ln(1 - a) + \ln \frac{m_b^2}{\nu^2} \right] + 288a^2 \ln a \ln(1 - a) \\ & \left. + 12a^2(18 - 8a + a^2) \ln a + 288a^2 \text{L}_2(a) \right\}. \end{aligned} \quad (\text{B.4})$$

B.3 Diagram VI

Applying Cutkosky rules and using the formulas of App. A, both three-particle cuts yield a complex result. In the sum, however, only the real parts contribute, for the cuts are complex conjugate to each other. One finds:

$$\begin{aligned}
\text{Im VI}^{(3\text{-part.})} = & -\frac{g_s^2}{192\pi^5 m_b^2} \int_{m_c^2}^{m_b^2} \frac{ds}{s^3} (s - m_c^2)^2 (m_b^2 - s)^2 \left\{ \left[2s^2 + (m_c^2 + m_b^2)s + 2m_c^2 m_b^2 \right] \right. \\
& \times \left\{ (s - m_c^2) \left[2\text{Re } \tilde{B}(m_c^2, s) - \text{Re } \tilde{K}(m_c^2, s) \right] + 2\text{Re } C(m_c^2, s) + 1 \right\} \\
& + s \left[2s^2 + (m_b^2 + m_c^2)s - m_c^2 m_b^2 \right] \text{Re } A(m_c^2, s) \\
& \left. + s \left[2s^2 + (4m_c^2 + m_b^2)s + 5m_c^2 m_b^2 \right] \text{Re } B(m_c^2, s) \right\}. \tag{B.5}
\end{aligned}$$

The pole of the function $C(m_b^2, s)$ in $D - 4$ cancels after addition of the counterterm diagram. Hence, only the UV finite pieces must be retained. Yet the subtraction of UV divergences has to be done with some care: counterterm diagrams must be added *before* performing the phase-space integration, which we explicitly carry out in *four* dimensions. This procedure has the advantage that one can ignore the evanescent operators. Note however that the three-particle cuts are IR divergent since they contain the functions $\tilde{K}(m_b^2, s)$ and $\tilde{B}(m_b^2, s)$.

With the help of App. A one can also check that the sum of the two four-particle cuts is

$$\begin{aligned}
\text{Im VI}^{(4\text{-part.})} = & -\frac{g_s^2}{192\pi^5 m_b^2} \int_{m_c^2}^{m_b^2} \frac{ds}{s^3} (m_b - s)^2 \left\{ \left[2s^2 + (m_c^2 + m_b^2)s + 2m_c^2 m_b^2 \right] \right. \\
& \times (s - m_c^2)^2 \left\{ (s - m_c^2) \left[\text{Re } \tilde{K}(m_c^2, s) - 2\text{Re } \tilde{B}(m_c^2, s) \right] + E'(m_c^2, s) \right\} \\
& - m_c^2 \left[s^2 + (2m_c^2 - m_b^2)s + 4m_c^2 m_b^2 \right] H(m_c^2, s) \\
& - \frac{sm_c^2}{2} (s + 2m_c^2)(s + 2m_b^2) \ln \frac{s}{m_c^2} - \frac{s - m_c^2}{12} \left[46s^3 \right. \\
& \left. \left. - (11m_c^2 - 20m_b^2)s^2 + m_c^2(19m_c^2 - 22m_b^2)s + 38m_c^4 m_b^2 \right] \right\}. \tag{B.6}
\end{aligned}$$

Obviously, the four-particle cuts are UV finite, because they do not involve any loop integration. Note that the IR divergences cancel in the sum of the three- and four-particle cuts. The result can be integrated with the help of App. A to yield:

$$\text{Im VI} = \frac{g_s^2 m_b^6}{9216\pi^5} \left\{ (1 - a)(61 - 165a - 390a^2 + 52a^3) + 4a^2(30 + 8a - a^2)\pi^2 \right.$$

$$\begin{aligned}
& -2(1-a^2) \left[25 - 272a + 25a^2 - 12(1-8a+a^2) \ln a \right] \ln(1-a) \\
& + 2a(12+18a+212a^2-19a^3) \ln a - 12a^2(18+8a-a^2) \ln^2 a - 12f_1(a) \ln \frac{m_b^2}{\mu^2} \\
& + 24(2-16a-30a^2+8a^3-a^4+12a^2 \ln a) L_2(a) + 864a^2 [\zeta(3) - L_3(a)] \}. \quad (\text{B.7})
\end{aligned}$$

B.4 Diagram VIII

Proceeding with diagram VIII along the same lines, one gets for the sum of the two three-particle cuts:

$$\begin{aligned}
\text{Im VIII}^{(3\text{-part.})} = & \frac{g_s^2}{32\pi^5 m_b^2} \int_{m_c^2}^{m_b^2} \frac{ds}{s} (m_b^2 - s)^2 (s - m_c^2)^2 \left\{ 2s [\text{Re } A(m_c^2, s) + \text{Re } B(m_c^2, s)] \right. \\
& \left. + (s - m_c^2) [2 \text{Re } \tilde{B}(m_c^2, s) - \text{Re } \tilde{K}(m_c^2, s)] + 8 \text{Re } C(m_c^2, s) + \frac{1}{2} \right\}, \quad (\text{B.8})
\end{aligned}$$

while the sum of the two four-particle cuts is

$$\begin{aligned}
\text{Im VIII}^{(4\text{-part.})} = & -\frac{g_s^2}{32\pi^5 m_b^2} \int_{m_c^2}^{m_b^2} \frac{ds}{s} (m_b^2 - s)^2 \left\{ (s - m_c^2)^3 [2 \text{Re } \tilde{B}(m_c^2, s) - \text{Re } \tilde{K}(m_c^2, s)] \right. \\
& \left. - (s - m_c^2)^2 E'(m_c^2, s) + (s - m_c^2) \frac{5s - m_c^2}{2} - 2m_c^2 s \ln \frac{s}{m_c^2} \right\}. \quad (\text{B.9})
\end{aligned}$$

Again, UV divergences are cancelled by the counterterm diagrams, whereas the IR divergences add to zero in the final sum. The latter one can be integrated to give:

$$\begin{aligned}
\text{Im VIII} = & \frac{g_s^2 m_b^6}{9216\pi^5} \left\{ (1-a)(-220+1374a+1863a^2-139a^3) - 4a^2(66+32a-a^2)\pi^2 \right. \\
& + 2(1-a) [37-379a-811a^2-11a^3-12(1+a)(1-8a+a^2) \ln a] \ln(1-a) \\
& - 2a(12-918a+596a^2+35a^3) \ln a + 12a^2(18+32a-a^2) \ln^2 a \\
& - 24(2-16a-66a^2-16a^3-a^4+12a^2 \ln a) L_2(a) \\
& \left. + 48f_1(a) \ln \frac{m_b^2}{\mu^2} + 864a^2 [L_3(a) - \zeta(3)] \right\}. \quad (\text{B.10})
\end{aligned}$$

B.5 Diagram X

With the same notations as above, we get for diagram X the following results:

$$\text{Im X}^{(3\text{-part.})} = \frac{g_s^2}{64\pi^5 m_b^2} \int_{m_c^2}^{m_b^2} \frac{ds}{s} (m_b^2 - s)^2 (s - m_c^2)^2 \left\{ 2s [A(m_b^2, s) + B(m_b^2, s)] \right.$$

$$+ 8C(m_b^2, s) + \frac{1}{2} + (m_b^2 - s)[\widetilde{K}(m_b^2, s) - 2\widetilde{B}(m_b^2, s)] \Big\}. \quad (\text{B.11})$$

Note that $A(m_b^2, s)$, $B(m_b^2, s)$, $C(m_b^2, s)$, $\widetilde{K}(m_b^2, s)$ and $\widetilde{B}(m_b^2, s)$ are now real functions because $s < m_b^2$. By adding the counterterm diagram one removes the UV divergent piece in $C(m_b^2, s)$, as it should be.

The four-particle cut yields

$$\begin{aligned} \text{Im } X^{(4\text{-part.})} = & -\frac{g_s^2}{64\pi^5 m_b^2} \int_{m_c^2}^{m_b^2} \frac{ds}{s} (s - m_c^2)^2 \Big\{ (m_b^2 - s)^3 [\widetilde{K}(m_b^2, s) - 2\widetilde{B}(m_b^2, s)] \\ & + (m_b^2 - s)^2 E(m_b^2, s) + (m_b^2 - s) H(m_b^2, s) - (m_b^2 - s) \frac{3s + m_b^2}{2} \\ & + s(s + m_b^2) \ln \frac{m_b^2}{s} \Big\}, \end{aligned} \quad (\text{B.12})$$

so that

$$\begin{aligned} \text{Im } [X + X^\dagger] = & \frac{g_s^2 m_b^6}{9216\pi^5} \Big\{ (1 - a)(-139 + 1863a + 1374a^2 - 220a^3) \\ & + 4(3 - 48a - 66a^2 + 16a^3 - 2a^4)\pi^2 - 864a^2 [L_3(a) - \zeta(3)] - 2(1 - a) \times \\ & \times [11 + 811a + 379a^2 - 37a^3 - 12(1 + a)(1 - 8a + a^2) \ln a] \ln(1 - a) \\ & + 2a(12 + 486a - 236a^2 + 13a^3 - 48a\pi^2) \ln a + 48f_1(a) \ln \frac{m_b^2}{\mu^2} \\ & + 24(1 + 16a + 66a^2 + 16a^3 - 2a^4 + 12a^2 \ln a) L_2(a) \Big\}. \end{aligned} \quad (\text{B.13})$$

Again the result is both UV and IR finite as it should be.

B.6 Diagram XI

$$\begin{aligned} \text{Im } XI^{(3\text{-part.})} = & \frac{g_s^2}{384\pi^5 m_b^2} \int_{m_c^2}^{m_b^2} \frac{ds}{s^3} (m_b^2 - s)^2 (s - m_c^2)^2 \Big\{ [2s^2 + (m_c^2 + m_b^2)s + 2m_c^2 m_b^2] \\ & \times \Big\{ (m_b^2 - s) [2\widetilde{B}(m_b^2, s) - \widetilde{K}(m_b^2, s)] - 2C(m_b^2, s) - 1 \Big\} \\ & - s [2s^2 + (m_b^2 + m_c^2)s - m_c^2 m_b^2] A(m_b^2, s) \\ & - s [2s^2 + (m_c^2 + 4m_b^2)s + 5m_c^2 m_b^2] B(m_b^2, s) \Big\}. \end{aligned} \quad (\text{B.14})$$

$A(m_b^2, s)$, $B(m_b^2, s)$, $C(m_b^2, s)$, $\widetilde{K}(m_b^2, s)$ and $\widetilde{B}(m_b^2, s)$ are real functions and the counterterm diagram cancels the pole of $C(m_b^2, s)$ in $D - 4$.

The four-particle cut is:

$$\begin{aligned} \text{Im XI}^{(4\text{-part.})} = & \frac{g_s^2}{384\pi^5 m_b^2} \int_{m_c^2}^{m_b^2} \frac{ds}{s^3} (s - m_c^2)^2 \left\{ \left[2s^2 + (m_c^2 + m_b^2)s + 2m_c^2 m_b^2 \right] (m_b^2 - s) \right. \\ & \times \left\{ (m_b^2 - s)^2 \left[\widetilde{K}(m_b^2, s) - 2\widetilde{B}(m_b^2, s) \right] + H(m_b^2, s) + (m_b^2 - s)E(m_b^2, s) \right\} \\ & + \frac{s^2}{2} \left[4s^2 + (2m_c^2 - m_b^2)s - 2m_c^2 m_b^2 \right] \ln \frac{m_b^2}{s} - \frac{m_b^2 - s}{12} \left[22s^3 \right. \\ & \left. \left. + (8m_c^2 - 11m_b^2)s^2 - m_b^2(22m_c^2 - 7m_b^2)s + 14m_c^2 m_b^4 \right] \right\}. \end{aligned} \quad (\text{B.15})$$

After integrating over s , the final sum can be written as:

$$\begin{aligned} \text{Im [XI + XI}^\dagger] = & \frac{g_s^2 m_b^6}{9216\pi^5} \left\{ (1 - a)(52 - 390a - 165a^2 + 61a^3) \right. \\ & - 4(3 - 24a - 30a^2 + 16a^3 - 2a^4)\pi^2 \\ & - 2(1 - a^2) \left[25 - 272a + 25a^2 + 12(1 - 8a + a^2) \ln a \right] \ln(1 - a) \\ & - 2a(12 - 18a - 236a^2 + 19a^3 - 48a\pi^2) \ln a - 12f_1(a) \ln \frac{m_b^2}{\mu^2} \\ & \left. + 24(-1 + 8a - 30a^2 - 16a^3 + 2a^4 - 12a^2 \ln a) \text{L}_2(a) + 864a^2 [\text{L}_3(a) - \zeta(3)] \right\}, \end{aligned} \quad (\text{B.16})$$

which again is explicitly UV and IR finite.

B.7 Diagram XII

For diagram XII only a four-particle cut is possible. Using the same techniques as before one finds:

$$\begin{aligned} \text{Im XII} = & -\frac{g_s^2}{64\pi^3 m_b^2} \int_{m_c^2}^{m_b^2} ds \left\{ \left[m_b^2 \rho_1^{(1)}(s) - 2\rho_2^{(1)}(s) \right] \left[4(m_b^2 - s)^2 \right. \right. \\ & \times \left\{ \ln \frac{m_b^2 - s}{m_b^2} - \frac{1}{2} \ln \frac{\lambda^2}{m_b^2} \right\} + s(2m_b^2 + 5s) \ln \frac{m_b^2}{s} - \frac{1}{2}(m_b^2 - s)(17m_b^2 - 3s) \left. \right] \\ & \left. + \rho_1^{(1)}(s) \left[-2sm_b^2(m_b^2 + 3s) \ln \frac{m_b^2}{s} + \frac{m_b^2 - s}{3}(s^2 + 28sm_b^2 - 5m_b^4) \right] \right\} \end{aligned}$$

$$\begin{aligned}
&= \frac{g_s^2 m_b^6}{18432 \pi^5} \left\{ 137 - 1024a - 324a^2 + 1216a^3 - 5a^4 + 96a^2 \pi^2 \right. \\
&\quad \left. - 24f_1(a) \left[2 \ln(1-a) - \ln \frac{\lambda^2}{m_b^2} \right] \right. \\
&\quad \left. - 12a^2(102 + 8a + 5a^2) \ln a - 576a^2 [\ln a \ln(1-a) + L_2(a)] \right\}. \tag{B.17}
\end{aligned}$$

The IR divergent logarithm of λ cancels the IR divergence in the sum of the diagrams II and II † , thus rendering an IR finite result. Similarly, the dependence on the renormalization scale μ cancels in the sum II + II † + V + XI + XI † + XII, as it should be for the semileptonic decay rate $\Gamma(b \rightarrow u\tau\bar{\nu})$.

It is important to emphasize that these results do not change under Fierz-transformations. This has been checked explicitly for the seven diagrams discussed in this appendix.

B.8 The Limit $m_c \rightarrow 0$

Here, we show that our results are well-defined in the limit $m_c \rightarrow 0$ and compare them with the corresponding quantities obtained in [6]. From (B.7), (B.10), (B.13) and (B.16) we get:

$$\text{Im VI}|_{m_c=0} = \frac{g_s^2 m_b^6}{768} \left(\frac{61}{12} - \ln \frac{m_b^2}{\mu^2} \right), \tag{B.18}$$

$$\text{Im VIII}|_{m_c=0} = \frac{g_s^2 m_b^6}{768} \left(-\frac{55}{3} + 4 \ln \frac{m_b^2}{\mu^2} \right), \tag{B.19}$$

$$\text{Im}[X + X^\dagger]|_{m_c=0} = \frac{g_s^2 m_b^6}{768} \left(-\frac{139}{12} + \pi^2 + 4 \ln \frac{m_b^2}{\mu^2} \right), \tag{B.20}$$

$$\text{Im}[XI + XI^\dagger]|_{m_c=0} = \frac{g_s^2 m_b^6}{768} \left(\frac{13}{3} - \pi^2 - \ln \frac{m_b^2}{\mu^2} \right). \tag{B.21}$$

In the notation of [6] this reads:

$$G_g = \frac{61}{12} - \ln \frac{m_b^2}{\mu^2}, \tag{B.22}$$

$$G_e = -\frac{55}{3} + 4 \ln \frac{m_b^2}{\mu^2}, \tag{B.23}$$

$$G_d = -\frac{139}{12} + \pi^2 + 4 \ln \frac{m_b^2}{\mu^2}, \tag{B.24}$$

$$G_f = \frac{13}{3} - \pi^2 - \ln \frac{m_b^2}{\mu^2}. \tag{B.25}$$

These results are scheme-dependent. In order to compare with [6], where the 't Hooft-Veltman scheme is used, we need to add the corresponding matching coefficients, B_d , B_e , B_f , B_g evaluated using NDR. Again in the notation of [6] one has:

$$B_d = B_e = 5, \quad B_f = B_g = \frac{1}{2} \quad (\text{B.26})$$

with $B = B_d + B_e + B_f + B_g = 11$, cf. (2.10). The agreement with [6] for the scheme-independent quantities $G_i + B_i$ is evident, which provides a non-trivial check of our calculation.

Appendix C

As mentioned in the text, the calculation of G_b and G_d is much simplified by using the results for the spectral densities of the vector correlation function, $1/\pi \text{Im} \Pi_{\mu\nu} = q_\mu q_\nu \rho_1^V + g_{\mu\nu} \rho_2^V$, Eq. (2.22), which can be obtained from [19] when the running mass is replaced by the pole mass; we have also calculated the spectral densities directly by using Cutkosky rules. Defining

$$\rho_i^V = 3 (\rho_i^{(1)} + C_F \rho_i^{(2)} + \dots), \quad (\text{C.1})$$

where $\rho_i^{(1)}$ is the tree-level and $\rho_i^{(2)}$ the next-to-leading order contribution, we find:

$$\rho_1^{(1)}(s) = \frac{1}{12\pi^2} \left(1 - \frac{m_c^2}{s}\right)^2 \left(1 + \frac{2m_c^2}{s}\right), \quad (\text{C.2})$$

$$\rho_2^{(1)}(s) = -\frac{1}{12\pi^2} s \left(1 - \frac{m_c^2}{s}\right)^2 \left(1 + \frac{m_c^2}{2s}\right), \quad (\text{C.3})$$

$$\begin{aligned} \rho_1^{(2)}(s) = & \frac{g_s^2}{192\pi^4} \left\{ 4 \left(1 - \frac{m_c^2}{s}\right)^2 \left(1 + \frac{2m_c^2}{s}\right) \left[\ln \frac{m_c^2}{s} \ln \left(1 - \frac{m_c^2}{s}\right) + 2\text{L}_2 \left(\frac{m_c^2}{s}\right) \right] \right. \\ & - 4 \left(1 + 2\frac{m_c^2}{s} - 2\frac{m_c^4}{s^2}\right) \ln \frac{m_c^2}{s} - 4 \left(1 - \frac{m_c^2}{s}\right)^2 \left(1 + 5\frac{m_c^2}{s} - \frac{3m_c^4}{2s^2}\right) \ln \frac{s - m_c^2}{m_c^2} \\ & \left. + 3 \left(1 - \frac{m_c^2}{s}\right) \left(1 + 3\frac{m_c^2}{s} - \frac{16m_c^4}{3s^2}\right) \right\}, \quad (\text{C.4}) \end{aligned}$$

$$\begin{aligned} \rho_2^{(2)}(s) = & -\frac{g_s^2}{192\pi^4} s \left\{ 4 \left(1 - \frac{m_c^2}{s}\right)^2 \left(1 + \frac{m_c^2}{2s}\right) \left[\ln \frac{m_c^2}{s} \ln \left(1 - \frac{m_c^2}{s}\right) + 2\text{L}_2 \left(\frac{m_c^2}{s}\right) \right] \right. \\ & - 4 \left(1 + \frac{m_c^2}{s}\right) \left(1 - \frac{m_c^2}{2s}\right) \ln \frac{m_c^2}{s} - 4 \left(1 - \frac{m_c^2}{s}\right)^2 \left(1 + \frac{5m_c^2}{4s}\right) \ln \frac{s - m_c^2}{m_c^2} \end{aligned}$$

$$+ 3 \left(1 - \frac{m_c^2}{s} \right) \left(1 - \frac{3m_c^2}{2s} - \frac{5m_c^4}{6s^2} \right) \Big\}. \quad (\text{C.5})$$

We repeat that the above spectral densities are expressed in terms of on-shell quark masses. In the limit $m_c \rightarrow 0$ one obtains

$$\rho_2^{(2)}(s) \Big|_{\text{massless}} = -s \rho_1^{(2)}(s) \Big|_{\text{massless}} = -\frac{g_s^2}{64\pi^4} s \quad (\text{C.6})$$

and $\Pi_{\mu\nu}$ becomes transverse, as it should.

Since for the calculation of diagram V, App. B.2., the part of $\rho_i^{(2)}$ corresponding to the light quark self-energy is needed separately, we give in addition to the sum, $\rho_i^{(2)}$, also the contributions of the single diagrams. All the three graphs are calculated in Feynman gauge and expressed in terms of the *running* $\overline{\text{MS}}$ mass whose relation to the pole mass is given by

$$m^{\text{pole}} = m_{\overline{\text{MS}}}(\mu) \left[1 + C_F \frac{g_s^2}{4\pi^2} \left(1 - \frac{3}{4} \ln \frac{m^2}{\mu^2} \right) \right]. \quad (\text{C.7})$$

We denote the spectral density of the light quark's self-energy diagram by ρ_i^{SEL} , that of the heavy quark by ρ_i^{SEH} and the gluon-exchange diagram by ρ_i^{EX} .

$$\begin{aligned} \rho_1^{\text{SEL}}(s) = & \frac{g_s^2}{1152\pi^4} \left[-\frac{s-m_c^2}{s} \left\{ 11 + 17 \frac{m_c^2}{s} - 34 \left(\frac{m_c^2}{s} \right)^2 \right\} - 6 \ln \frac{s}{m_c^2} \right. \\ & \left. + 6 \left(\frac{s-m_c^2}{s} \right)^2 \frac{2m_c^2+s}{s} \left\{ \ln \frac{m_c^2}{\mu^2} + 2 \ln \frac{s-m_c^2}{m_c^2} \right\} \right], \end{aligned} \quad (\text{C.8})$$

$$\begin{aligned} \rho_2^{\text{SEL}}(s) = & \frac{g_s^2}{2304\pi^4} \left[(s-m_c^2) \left\{ 28 - 5 \frac{m_c^2}{s} - 17 \left(\frac{m_c^2}{s} \right)^2 \right\} + 6(2s-3m_c^2) \ln \frac{s}{m_c^2} \right. \\ & \left. - 6 \left(\frac{s-m_c^2}{s} \right)^2 (2m_c^2+s) \left\{ \ln \frac{m_c^2}{\mu^2} + 2 \ln \frac{s-m_c^2}{m_c^2} \right\} \right], \end{aligned} \quad (\text{C.9})$$

$$\begin{aligned} \rho_1^{\text{SEH}}(s) = & \frac{g_s^2}{1152\pi^4} \left[-\frac{s-m_c^2}{s} \left\{ 11 - 55 \frac{m_c^2}{s} + 362 \left(\frac{m_c^2}{s} \right)^2 \right\} + 30 \ln \frac{s}{m_c^2} \right. \\ & + 6 \frac{s-m_c^2}{s} \left\{ 1 + \frac{m_c^2}{s} + 34 \left(\frac{m_c^2}{s} \right)^2 \right\} \ln \frac{m_c^2}{\mu^2} \\ & \left. - 24 \left(\frac{s-m_c^2}{s} \right)^2 \left(1 + 2 \frac{m_c^2}{s} \right) \ln \frac{s-m_c^2}{m_c^2} \right], \end{aligned} \quad (\text{C.10})$$

$$\begin{aligned}
\rho_2^{\text{SEH}}(s) = & \frac{g_s^2}{2304\pi^4} \left[(s - m_c^2) \left\{ 28 + 157 \frac{m_c^2}{s} + 181 \left(\frac{m_c^2}{s} \right)^2 \right\} - 6(10s + 3m_c^2) \ln \frac{s}{m_c^2} \right. \\
& - 6(s - m_c^2) \left\{ 2 + 17 \frac{m_c^2}{s} + 17 \left(\frac{m_c^2}{s} \right)^2 \right\} \ln \frac{m_c^2}{\mu^2} \\
& \left. + 24 \left(\frac{s - m_c^2}{s} \right)^2 (2s + m_c^2) \ln \frac{s - m_c^2}{m_c^2} \right], \tag{C.11}
\end{aligned}$$

$$\begin{aligned}
\rho_1^{\text{EX}}(s) = & \frac{g_s^2}{288\pi^4} \frac{s - m_c^2}{s} \left[\frac{s - m_c^2}{s} \left\{ 2 \left(5 + 7 \frac{m_c^2}{s} \right) - 3 \left[1 + 8 \frac{m_c^2}{s} - 3 \left(\frac{m_c^2}{s} \right)^2 \right] \ln \frac{s - m_c^2}{m_c^2} \right. \right. \\
& - 3 \left(1 + 2 \frac{m_c^2}{s} \right) \left[\ln \frac{m_c^2}{\mu^2} + 2 \ln \frac{s}{m_c^2} \ln \frac{s - m_c^2}{s} - 4\text{L}_2 \left(\frac{m_c^2}{s} \right) \right] \left. \right\} \\
& \left. + 12 \frac{m_c^2}{s} \ln \frac{s}{m_c^2} \right], \tag{C.12}
\end{aligned}$$

$$\begin{aligned}
\rho_2^{\text{EX}}(s) = & \frac{g_s^2}{1152\pi^4} \left[-(s - m_c^2) \left\{ 46 - 23 \frac{m_c^2}{s} - 5 \left(\frac{m_c^2}{s} \right)^2 \right\} + 6m_c^2 \left(1 + 2 \frac{m_c^2}{s} \right) \ln \frac{s}{m_c^2} \right. \\
& + 6 \left(\frac{s - m_c^2}{s} \right)^2 \left\{ 2(s + 2m_c^2) \ln \frac{s - m_c^2}{m_c^2} + (2s + m_c^2) \left[\ln \frac{m_c^2}{\mu^2} \right. \right. \\
& \left. \left. + 2 \ln \frac{s}{m_c^2} \ln \frac{s - m_c^2}{s} - 4\text{L}_2 \left(\frac{m_c^2}{s} \right) \right] \right\} \left. \right]. \tag{C.13}
\end{aligned}$$

References

- [1] I. Bigi *et al.*, Phys. Rev. Lett. **71** (1993) 496;
A. Manohar and M.B. Wise Phys. Rev. D **49** (1994) 1310;
B. Blok *et al.*, Phys. Rev. D **49** (1994) 3356;
T. Mannel, Nucl. Phys. **B413** (1994) 396;
A.F. Falk, M. Luke and M. Savage, Phys. Rev. D **49** (1994) 3367
- [2] I. Bigi, N. Uraltsev and A. Vainshtein, Phys. Lett. B **293** (1992) 430; Erratum *ibid.* **297** (1993) 477
- [3] N. Cabibbo and L. Maiani, Phys. Lett. B **79** (1978) 109
- [4] R.E. Behrends, R.J. Finkelstein and A. Sirlin, Phys. Rev. **101** (1956) 866;
S.M. Berman, Phys. Rev. **112** (1958) 267;
T. Kinoshita and A. Sirlin, Phys. Rev. **113** (1959) 1652
- [5] G. Altarelli *et al.*, Nucl. Phys. **B187** (1981) 461
- [6] G. Buchalla, Nucl. Phys. **B391** (1993) 501
- [7] Q. Hokim and X.Y. Pham, Phys. Lett. B **122** (1983) 297; Ann. Phys. **155** (1984) 202
- [8] Y. Nir, Phys. Lett. B **221** (1989) 184
- [9] D.J. Broadhurst and A.G. Grozin, Phys. Lett. B **274** (1992) 421;
E. Bagan *et al.*, Phys. Lett. B **278** (1992) 457
- [10] H. Albrecht *et al.* (ARGUS Collab.), Phys. Lett. B **318** (1993) 397;
M. Athanas *et al.* (CLEO Collab.), Preprint CLNS-94-1286 (hep-ex/9406004);
R. Patterson, *Weak and Rare Decays*, Rapporteur Talk at ICHEP 94, Glasgow, 20–27 July 1994
- [11] G. Altarelli and S. Petrarca, Phys. Lett. B **261** (1991) 303
- [12] W.F. Palmer and B. Stech, Phys. Rev. D **48** (1993) 4174
- [13] I. Bigi *et al.*, Phys. Lett. B **323** (1994) 408
- [14] A.F. Falk, M.B. Wise and I. Dunietz, CALTEC Preprint CALT-68-1933 (1994) (hep-ph/9405346)
- [15] D. Buskulic *et al.* (ALEPH Collab.), Phys. Lett. B **298** (1993) 479;
M. Acciarri *et al.* (L3 Collab.), Phys. Lett. B **332** (1994) 201;
A.F. Falk *et al.*, Phys. Lett. B **326** (1994) 145;
L. Koyrakh, Phys. Rev. D **49** (1994) 3379;
S. Balk *et al.*, Mainz Preprint MZ-TH/93-32 (hep-ph/9312220)

- [16] A.J. Buras and P.H. Weisz, Nucl. Phys. **B333** (1990) 66
- [17] M. Jamin and A. Pich, Preprint CERN-TH.7151/94 (1994) (hep-ph/9402363)
- [18] S. Herrlich and U. Nierste, TU München Preprint TUM-T31-66/94 (in preparation)
- [19] S.C. Generalis, J. Phys. G **16** (1990) 785
- [20] J.L. Cortes, X.Y. Pham and A. Tounsi, Phys. Rev. D **25** (1982) 188
- [21] I. Bigi *et al.*, Minneapolis Preprint TPI-MINN-94/25-T (hep-ph/9407296)
- [22] P. Ball and V.M. Braun, Phys. Rev. D **49** (1994) 2472
- [23] M. Neubert, Phys. Lett. B **322** (1994) 419
- [24] I. Bigi *et al.*, Minneapolis Preprint TPI-MINN-94/12-T (hep-ph/9405410)
- [25] I. Bigi *et al.*, Phys. Rev. D **50** (1994) 2234;
M. Beneke and V.M. Braun, MPI München Preprint MPI-PhT/94-9 (hep-ph/9402364) (to appear in Nucl. Phys. **B**);
M. Beneke, V.M. Braun and V.I. Zakharov, MPI München Preprint MPI-PhT/94-18 (hep-ph/9405304)
- [26] M. Aguilar-Benitez *et al.* (Particle Data Group), Phys. Rev. D **50** (1994) 1173
- [27] World average presented by S. Bethke at the QCD 94 conference, Montpellier, 7–13 July 1994
- [28] E. Bagan *et al.*, TU München Preprint TUM-T31-68/94 (in preparation)
- [29] H. Pietschmann, *Weak interactions – Formulæ, Results and Derivations*, Wien 1983

Figures

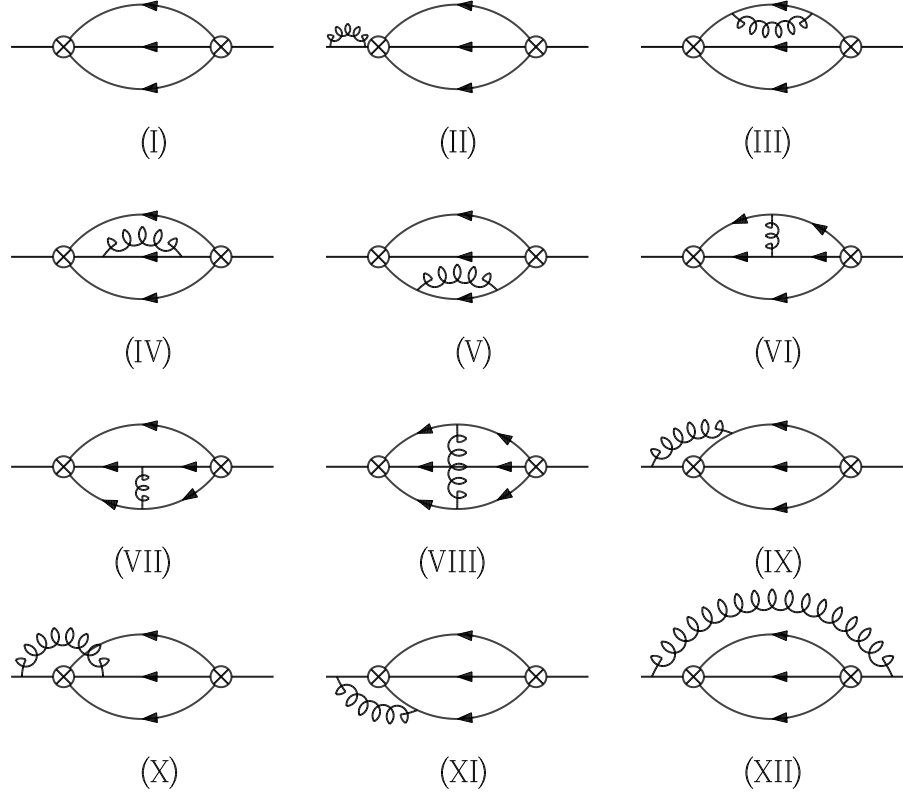


Figure 1: The diagrams contributing to the forward-scattering amplitude Eq. (2.16) up to order α_s . The crossed circles denote insertions of the operator \mathcal{O} . Of the three internal quark lines, the upper one denotes the c quark, the lower one the d quark, and the middle one the u antiquark.

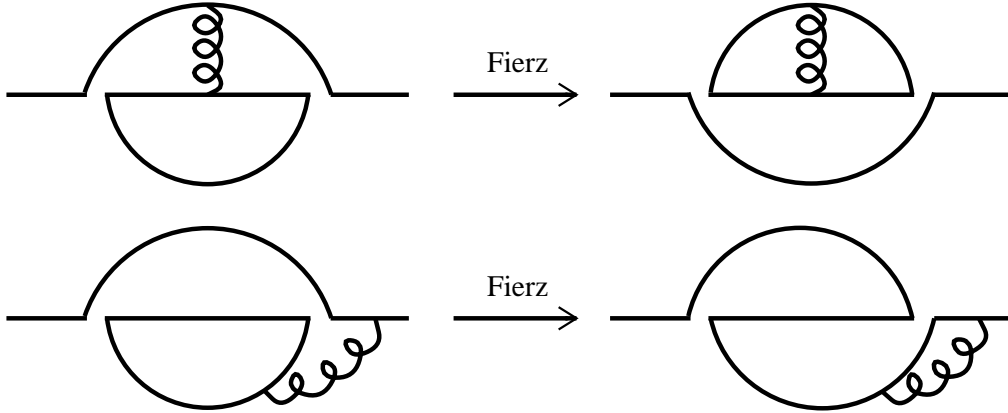


Figure 2: Illustration of the effect of Fierz-transformations on the diagrams VI and XI. In contrast to the left-hand side diagrams, the ones on the right-hand side are well defined in NDR.

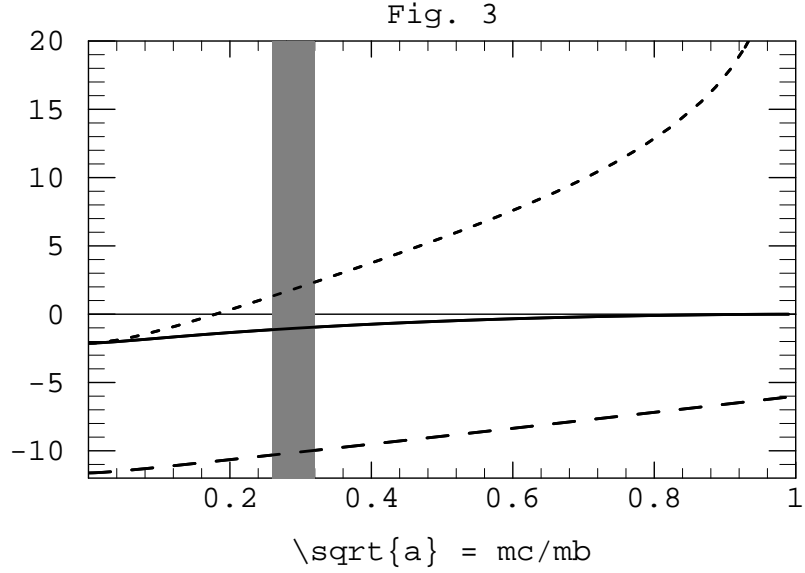


Figure 3: Radiative corrections from the different combinations of operator insertions as defined in Eq. (5.1) as functions of m_c/m_b for $\mu = m_b$: short dashes: c_{11} , long dashes: c_{12} , solid line: c_{22} . The grey bar indicates the range of realistic values of m_c/m_b . The numerical values are tabulated in Tab. 4.

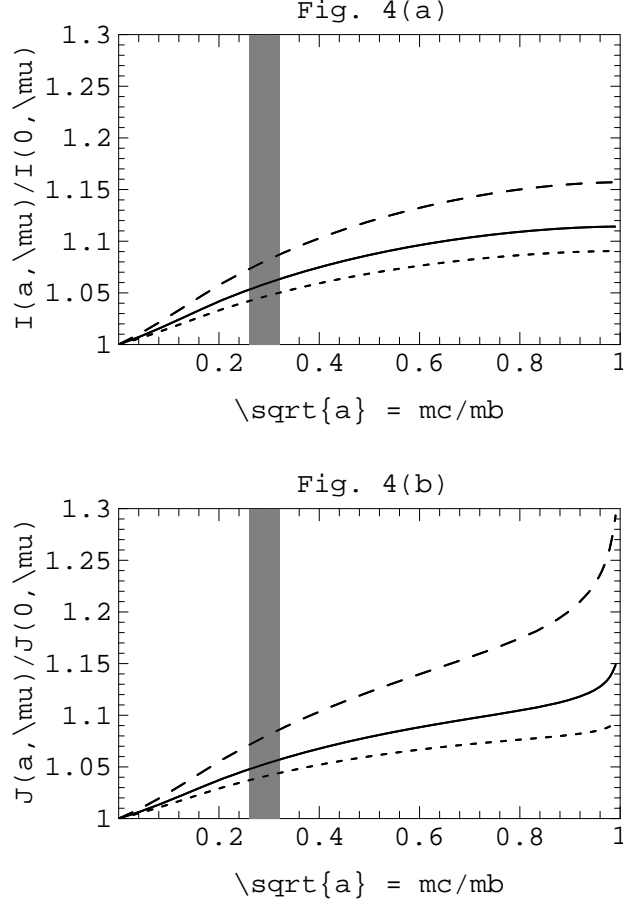


Figure 4: (a) The next-to-leading order correction $I(a, \mu)$ to $\Gamma(b \rightarrow ce\bar{\nu})$, Eq. (5.4), as function of $\sqrt{a} = m_c/m_b$, normalized to one at $m_c = 0$, for $\alpha_s(m_Z) = 0.117$ and three different choices of the renormalization scale: solid line: $\mu = m_b$, long dashes: $\mu = m_b/2$, short dashes: $\mu = 2m_b$. (b) The next-to-leading order correction $J(a, \mu)$ to $\Gamma(b \rightarrow c\bar{u}d)$, Eq. (5.2), as function of $\sqrt{a} = m_c/m_b$, normalized to one at $m_c = 0$ and using the same parameters as in (a). The grey bar indicates the range of realistic values of m_c/m_b .

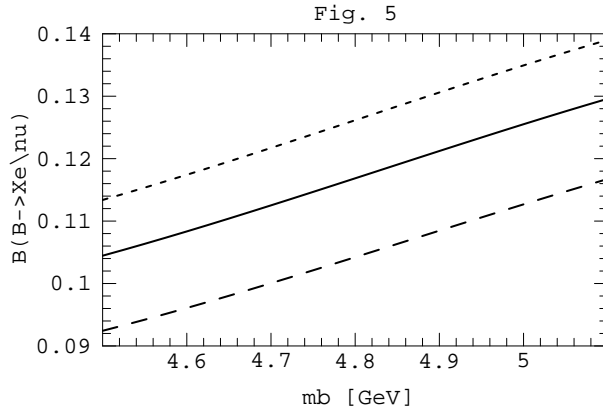


Figure 5: The semileptonic branching ratio of the B meson including non-perturbative corrections as a function of m_b with $m_b - m_c$ fixed by HQET and $\alpha_s(m_Z) = 0.117$. The three lines correspond to three different choices of the renormalization scale: solid line: $\mu = m_b$, long dashes: $\mu = m_b/2$, short dashes: $\mu = 2m_b$.

Tables

| Diagram No. | $\mathcal{O}_1 \otimes \mathcal{O}_1$ | $\mathcal{O}_1 \otimes \mathcal{O}_2$ | $\mathcal{O}_2 \otimes \mathcal{O}_2$ |
|-------------|---------------------------------------|---------------------------------------|---------------------------------------|
| I | 3 | 1 | 3 |
| II | $3 C_F$ | C_F | $3 C_F$ |
| III | $3 C_F$ | C_F | $3 C_F$ |
| IV | $3 C_F$ | C_F | $3 C_F$ |
| V | $3 C_F$ | C_F | $3 C_F$ |
| VI | $3 C_F$ | C_F | 0 |
| VII | 0 | C_F | $3 C_F$ |
| VIII | 0 | C_F | 0 |
| IX | 0 | C_F | $3 C_F$ |
| X | 0 | C_F | 0 |
| XI | $3 C_F$ | C_F | 0 |
| XII | $3 C_F$ | C_F | $3 C_F$ |

Table 1: The colour-factors multiplying the diagrams shown in Fig. 1 for all possible combinations of operator insertions. For an arbitrary number of colours N_c , C_F equals $(N_c^2 - 1)/(2N_c)$.

| $\sqrt{a} = m_c/m_b$ | 0 | 0.1 | 0.2 | 0.3 | 0.4 | ≈ 0.5 |
|----------------------|-------|-------|-------|-------|-------|--|
| $H_a(a)$ | -3.62 | -3.22 | -2.71 | -2.21 | -1.75 | |
| $H_b(a)$ | 1.5 | 2.43 | 4.20 | 6.70 | 10.5 | $\frac{739}{70} + \frac{2}{3} \pi^2 - 15 \ln 2 - 3 \ln \left(\frac{1}{4} - a \right)$ |
| $H_c(a)$ | -3.62 | -3.58 | -3.44 | -3.11 | -2.16 | |
| $H_d(a)$ | 1.5 | 3.37 | 6.46 | 12.8 | 24.3 | |

Table 2: Numerical values of the functions H_x defined in Sec. 4.

| $\sqrt{a} = m_c/m_b$ | 0 | 0.1 | 0.2 | 0.3 | 0.4 |
|-----------------------------------|---------|-------------|-------------|-------------|-------------|
| $\Gamma(b \rightarrow c\bar{c}s)$ | 1.112 | 1.005 | 0.671 | 0.283 | 0.043 |
| $\times 64\pi^3/(G_F^2 m_b^5)$ | ± 0 | ± 0.006 | ± 0.008 | ± 0.005 | ± 0.001 |

Table 3: The decay rate $\Gamma(b \rightarrow c\bar{c}s)$ in units of $G_F^2 m_b^5/(64\pi^3)$ as function of m_c/m_b for $\mu = m_b$ and $\alpha_s(m_Z) = 0.117$. The error denotes the uncertainty in the radiative corrections to the free quark decay.

| $\sqrt{a} = m_c/m_b$ | c_{11} | $c_{12}(\mu = m_b)$ | c_{22} |
|----------------------|--|------------------------|------------------------|
| 0 | $\frac{31}{4} - \pi^2$ | $-\frac{7}{4} - \pi^2$ | $\frac{31}{4} - \pi^2$ |
| 0.1 | -1.2 | -11. | -1.8 |
| 0.2 | 0.32 | -11. | -1.3 |
| 0.3 | 2.0 | -10. | -1.0 |
| 0.4 | 3.8 | -9.5 | -0.73 |
| 0.5 | 5.6 | -8.9 | -0.51 |
| 0.6 | 7.6 | -8.4 | -0.33 |
| 0.7 | 9.9 | -7.8 | -0.20 |
| 0.8 | 13. | -7.2 | -0.094 |
| 0.9 | 17. | -6.6 | -0.027 |
| 1 | $\frac{147}{10} - \frac{2}{3}\pi^2 - 6 \ln(1-a)$ | -6 | 0 |

Table 4: Numerical values of the coefficients c_{ij} defined in (5.1).

| $\alpha_s(m_Z)$ | Parton Model [11] | HQE [13] | HQE [this work] |
|-----------------|-------------------|----------|-----------------|
| 0.110 | 0.132 | 0.130 | 0.121 |
| 0.117 | 0.128 | 0.126 | 0.116 |
| 0.124 | 0.124 | 0.121 | 0.111 |

Table 5: $B(B \rightarrow X e \nu)$ in different models depending on $\alpha_s(m_Z)$. Input parameters: $m_b = 4.8 \text{ GeV}$, $m_c = 1.3 \text{ GeV}$, which corresponds to $\lambda_1 = -0.6 \text{ GeV}^2$. In the phase-space factor of $\Gamma(b \rightarrow c\bar{c}s)$ we use $m_s = 0.2 \text{ GeV}$. HQE is short-hand for heavy quark expansion.